공학박사 학위논문

# Physiological Information Analysis Using Unobtrusive Sensors:

## BCG from Load-Cell Based Infants' Bed and ECG from Patch Electrode

# 무구속 센서를 이용한 생체정보의 분석:

## 로드셀을 이용한 영유아 심탄도 측정 및 패치형 전극을 이용한 심전도 측정

**2016년 8월**


서울대학교 대학원

협동과정 바이오엔지니어링 전공

이 원 규

# Physiological Information Analysis Using Unobtrusive Sensors:

## BCG from Load-Cell Based Infants' Bed and ECG from Patch Electrode

# 무구속 센서를 이용한 생체정보의 분석:

## 로드셀을 이용한 영유아 심탄도 측정 및 패치형 전극을 이용한 심전도 측정

지도교수 박 광 석

이 논문을 공학박사 학위논문으로 제출함

2016년 5월


서울대학교 대학원

협동과정 바이오엔지니어링 전공

이 원 규


이원규의 공학박사 학위논문을 인준함

2016년 6월

| | | |
|---|---|---|
| 위 원 장 | Sungwan Kim | (인) |
| 부 위 원 장 | 박 광 석 | (인) |
| 위 원 | 최 진 욱 | (인) |
| 위 원 | 이 태 수 | (인) |
| 위 원 | 임 용 규 | (인) |

**Ph.D. Dissertation**

# Physiological Information Analysis Using Unobtrusive Sensors:

## BCG from Load-Cell Based Infants' Bed and ECG from Patch Electrode

**August 2016**

**Interdisciplinary Program in Bioengineering**

**The Graduate School**

**Seoul National University**

**Wonkyu Lee**

# Physiological Information Analysis Using Unobtrusive Sensors:

## BCG from Load-Cell Based Infants' Bed and ECG from Patch Electrode

*Academic adviser* **Kwangsuk Park**

**Submitting a Ph.D. Dissertation**

**May 2016**

**Interdisciplinary Program in Bioengineering**
**The Graduate School**
**Seoul National University**

**Wonkyu Lee**

**Confirming the Ph.D. Dissertation written by Wonkyu Lee**

**June 2016**

| | |
|---|---|
| Chair | *Kim, Sungwan, Ph.D.* |
| Vice Chair | *Park, Kwangsuk, Ph.D.* |
| Examiner | *Choi, Jinwook, M.D. & Ph.D.* |
| Examiner | *Lee, Taesoo, Ph.D.* |
| Examiner | *Lim, Yong-gyu, Ph.D.* |

## Abstract

# Physiological Information Analysis Using Unobtrusive Sensors:

## BCG from Load-Cell Based Infants' Bed and ECG from Patch Electrode

Wonkyu Lee

Interdisciplinary Program in Bioengineering

The Graduate School

Seoul National University

The aging population, chronic diseases, and infectious diseases are major challenges for our current healthcare system. To address these unmet healthcare needs, especially for the early prediction and treatment of major diseases, acquiring physiological information of different types has emerged as a promising interdisciplinary research area. Unobtrusive sensing techniques are instrumental in constructing a routine health management system, because they can be incorporated in daily life without confining individuals or causing any discomfort. This dissertation is dedicated to summarizing our research on monitoring of cardiorespiratory activities by means of unobtrusive sensing methods. Ballistocardiography and electrocardiography, which record the activity of the cardiorespiratory

system with respect to mechanical or electrical characteristics, are both being actively investigated as important physiological signal measurement that provide the information required to monitor human health states. This research was carried out to evaluate the feasibility of new application methods of unobtrusive sensing that not been investigated significantly in previous investigations. We also tried to incorporate improvement essential for bringing these technologies to practical use.

Our first device is a non-confining system for monitoring the physiological information of infants using ballistocardiography technology. Techniques to observe continuous biological signals without confinement may be even more important for infants since they could be used effectively to detect respiratory distress and cardiac abnormalities. We also expect to find extensive applications in the field of sleep research for analyzing sleep efficiency and sleep patterns of infants. Specifically, the sleep of infants is closely related to their health, growth, and development. Children who experience abnormal sleep and activity rhythms during their early infantile period are more prone to developing sleep-related disorders in late childhood, which are also more difficult to overcome. Therefore, studying their sleep characteristics is extremely important. Although ballistocardiography technology seems to represent a possible solution to overcome the limitations of conventional physiological signal monitoring, most studies investigating the application of these methods have focused on adults, and few have been focused on infants. To verify the usefulness of ballistocardiogram (BCG)-based physiological measurement in infants, we describe a load-cell based signal monitoring bed and assess an algorithm to estimate heartbeat and respiratory information. Four infants participated in 13 experiments. As a reference signal, electrocardiogram (ECG) and

respiration signals were simultaneously measured using a commercial device. The proposed automatic algorithm then selected the optimal sensor from which to estimate the heartbeat and respiratory information. The results from the load-cell sensor signals were compared with those of the reference signals, and the heartbeat and respiratory information were found to have average performance errors of 2.55% and 2.66%, respectively. We believe that our experimental results verify the feasibility of BCG-based measurements in infants.

Next, we developed a small, light, ECG monitoring device with enhanced portability and wearability, with software that contains a peak detection algorithm for analyzing heart rate variability (HRV). A mobile ECG monitoring system, which can assess an individual's condition efficiently during daily life activities, could be beneficial for management of their health care. A portable ECG monitoring patch with a minimized electrode array pad, easily attached to a person's chest, was developed. To validate the device's performance and efficacy, signal quality analysis in terms of robustness under motion, and HRV results obtained under stressful conditions were assessed by comparing the developed device with a commercially available ECG device. The R-peak detection results obtained with the device exhibited a sensitivity of 99.29%, a positive predictive value of 100.00%, and an error of 0.71%. The device also exhibited less motional noise than conventional ECG recording, being stable up to a walking speed of 5 km/h. When applied to mental stress analysis, the device evaluated the variation in HRV parameters in the same way as a reference ECG signal, with very little difference. Thus, our portable ECG device with its integrated minimized electrode patch carries promise as a form of ECG measurement technology that can be used for daily health monitoring.

There is currently an increased demand for continuous health monitoring systems with unobtrusive sensors. All of the experimental results in this dissertation verify the feasibility of our unobtrusive cardiorespiratory activity monitoring system. We believe that the proposed device and algorithm presented here are essential prerequisites toward substantiating the utility of unobtrusive physiological measurements. We also expect this system can help users better understand their state of health and provide physicians with more reliable data for objective diagnosis.

**Keywords:** ubiquitous healthcare; unobtrusive sensor, physiological information analysis, portable ECG monitoring patch, ballistocardiography technology for infants, heart rate variability, peak detection algorithm, automatic optimal sensor selection algorithm, stress assessment

**Student Number: 2011-30297**

# Table of Contents

**Chapter 1. Introduction .....1**

1.1. Cardiorespiratory signal and its related physiological information .....2

1.1.1. Electrocardiogram .....2

1.1.2. Ballistocardiogram .....3

1.1.3. Respiration .....4

1.1.4. Heart rate and breathing rate .....5

1.1.5. Variability analysis of heart and respiratory rate .....5

1.2. Unobtrusive sensing methods for continuous physiological monitoring .....6

1.3. Outline of the dissertation .....9

**Chapter 2. Development of sensor device for unobtrusive physiological signal measurement .....13**

2.1. Unobtrusive BCG measurement device for infants' health monitoring .....13

2.1.1. Specifications of the device .....17

2.1.2. Signal processing in hardware .....18

2.1.3. Performance of the device .....21

2.2. Unobtrusive ECG measurement device for health monitoring in daily life .....25

2.2.1. Specifications of the device .....26

2.2.2. Signal processing in hardware .....28

2.2.3. Performance of the device ..... 30

**Chapter 3. Development of algorithm for physiological information analysis from unobtrusively measured signal .....35**

3.1. Algorithm for automatically analyzing unobtrusively measured BCG signal .....35

3.1.1. Process flow of the algorithm ..... 36

3.1.1.1. Pre-processing of the data ..... 38

3.1.1.2. Signal quality check and sensor selection ..... 42

3.1.2. Performance evaluation ..... 47

3.1.2.1. Subjects and experimental method ..... 47

3.1.2.2. Results ..... 52

3.2. Algorithm for automatically analyzing unobtrusively measured ECG signal .....57

3.2.1. Process flow of the algorithm ..... 57

3.2.2. Performance evaluation ..... 60

3.2.2.1. Subjects and experimental method ..... 60

3.2.2.2. Results ..... 61

3.3. HRV analysis for processing unobtrusively measured signals .....63

3.3.1. Optimum HRV algorithm selection in data missing simulation ..... 64

3.3.2. Stress assessment using HRV parameters ..... 67

**Chapter 4. Discussion .....71**

**Chapter 5. Conclusion .....79**

**Reference .....81**

**Abstract in Korean .....89**

**Appendix .....93**

# List of Tables


Table 1. Technical specifications of load-cell sensor ..... 17

Table 2. Physical information about the participating subjects and experimental time ..... 48

Table 3. Performance evaluation results with respect to the beat locations in HR analysis ..... 52

Table 4. Performance evaluation results with respect to the beat locations in BR analysis ..... 53

Table 5. Comparison of HRs calculated from commercial device and proposed device ..... 54

Table 6. Comparison of BRs calculated from commercial device and proposed device ..... 55

Table 7. Performance summary of other related works ..... 56

Table 8. Performance evaluation of proposed RS-based peak-detection method ..... 62

Table 9. Performance summary of other related works ..... 63

Table 10. Changes of HRV parameters under stressful conditions ... 70

Table 11. Results of LF/HF ratio using various spectral analysis methods ..... 70

# List of Figures


Figure 1. The sequence of heart activities related to the deflection wave of an ECG ..... 2

Figure 2. Typical ECG and BCG waveforms ..... 3

Figure 3. Typical waveforms of respiratory signal ..... 4

Figure 4. Examples of seamless monitoring of physiological information in daily life ..... 8

Figure 5. (a) Design of physiological signal monitoring bed for infants; (b) Experimental setup of signal acquisition system ..... 16

Figure 6. (a) Schematic diagram of signal processing circuit for the load-cell sensor; (b) Simulation results of frequency response of signal processing circuit ..... 20

Figure 7. Setup for demonstrating the system's frequency response.... ..... 21

Figure 8. Results for resonant frequency of the load-cell integrated bed system ..... 22

Figure 9. Simultaneous recordings of (a) ECG, (b) respiration signal, and (d) – (f) raw signals from four load-cell sensors, (g) typical BCG waveform, and (h) waveform features of the BCG signal in our study. ..... 24

Figure 10. Smart ECG monitoring device ..... 27

Figure 11. Architecture of developed device ..... 29

Figure 12. Comparison of SNR between commercial and developed devices under conditions representing daily activities: (a) mean data, (b) box-plot comparison, (c) frequency distribution table ..... 32

Figure 13. Examples of ECG signals recorded using a commercial device (blue dotted line) and the developed device (black line): 5 km/h data for (a) subject 4, (b) subject 6, (c) subject 10, (d) subject 12 ..... 33
Figure 14. Flowchart of the proposed algorithms for automatic (a) HR and (b) BR analysis . ..... 37
Figure 15. Pre-processing steps for the HR analysis ..... 39
Figure 16. Pre-processing steps for the BR analysis ..... 41
Figure 17. Signal quality check based on the THV-S and sensor selection for HR analysis ..... 43
Figure 18. Signal quality check based on the THV-S and sensor selection for BR analysis ..... 44
Figure 19. Partial example of operating algorithm in HR analysis ... 46
Figure 20. Manually annotated peak locations and automatic peak detection results of the load-cell sensor signal obtained by the developed algorithm in (a) HR analysis and (b) BR analysis ..... 50
Figure 21. Flowchart of RS-based peak detection algorithm ..... 57
Figure 22. Results of the missing-data HRV simulation study ..... 66
Figure 23. Stress inducing tasks (a) Stroop test (b) mental arithmetic task ..... 68
Figure 24. Comparison of HRV parameters under stressful conditions ..... 69

# List of Abbreviations

**ECG** Electrocardiogram

**BCG** Ballistocardiogram

**PPG** Photoplethysmogram

**SCG** Seismocardiogram

**HR** Heart Rate

**BR** Breathing Rate

**HRV** Heart Rate Variability

**RRV** Respiratory Rate Variability

**ANS** Autonomic Nervous System

**SNR** Signal to Noise Ratio

**PSD** Power Spectral Density

**TP** True Positive

**FP** False Positive

**FN** False Negative

**Se** Sensitivity

**PPV** Positive Predictive Value

**Dr** Detection Rate

**Er** Error

# Chapter 1

# Introduction

Health has become a constant concern for people in modern society, given their irregular lifestyles and high levels of stress. This has manifested itself in the shift from the trend of striving to diagnose and treat diseases as early as possible to the more recent trend of constantly keeping track of an individual's physiological information and helping to maintain their health so that they do not develop diseases (41).

Ubiquitous healthcare (U-healthcare) is a technique that responds to the needs of modern people. By integrating information technology and medical technology, U-healthcare provides healthcare and medical services without the limitations of time or space and helps improve and manage the health of people in modern society. Through the application of this technology, people can constantly monitor their health and seek appropriate medical care when needed (37).

## 1.1. Cardiorespiratory signal and its related physiological information

### 1.1.1. Electrocardiogram

The electrocardiogram (ECG) is a signal that represents the electrical activity of the heart. Figure 1 shows the sequence of depolarization and repolarization of the heart following ECG tracing from the SA node, through the AV node and the His-Purkinje system to the contraction that pumps blood (21). Since an ECG reflects the rhythmic electrical depolarization and repolarization of the atria and ventricles, its shape, time interval, and amplitude provide useful information about the current state of the heart. The ECG waveform is characterized by its main waves: P, QRS complex, and T. The most important wave is the QRS complex, which characterizes the ventricular depolarizations (66). P and T waves correspond to atrial depolarization and ventricular repolarization, respectively.

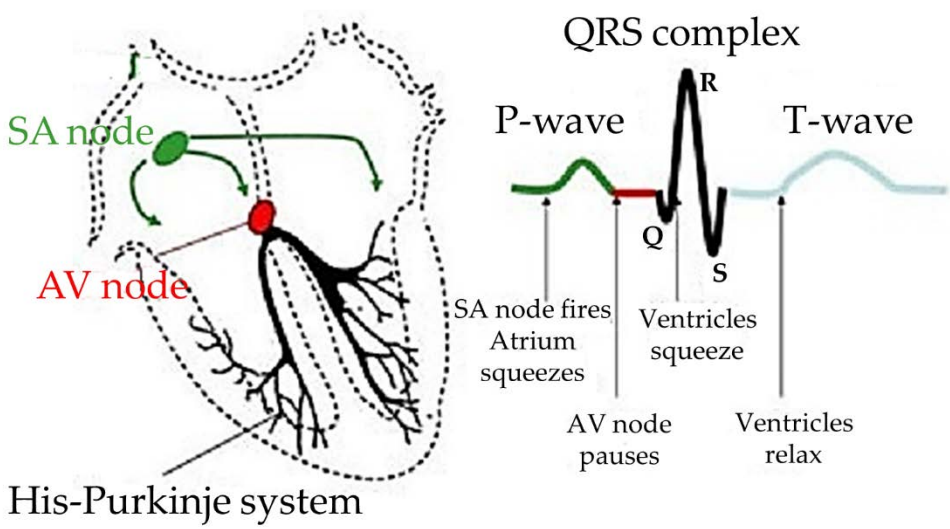


**Figure 1.** The sequence of heart activities related to the deflection waves of an ECG (21).

### 1.1.2. Ballistocardiogram

The ballistocardiogram (BCG) is based on the mechanical activity of the heart. At every heartbeat, the blood travelling along the vascular tree produces changes in the body's center of mass. Body micro-movements are then generated by the recoil forces to maintain overall momentum. Ballistocardiography is non-invasive technique that measure these reactional motions, as displacement, velocity, or acceleration signals (26). The waves of a BCG may be separated into three major groups: the pre-systolic, the systolic, and the diastolic. The waves were named with capital letters G through O. The I, and J waves are referred to as ejection waves. Figure 2 shows typical ECG and BCG waveforms with main characteristic peaks.

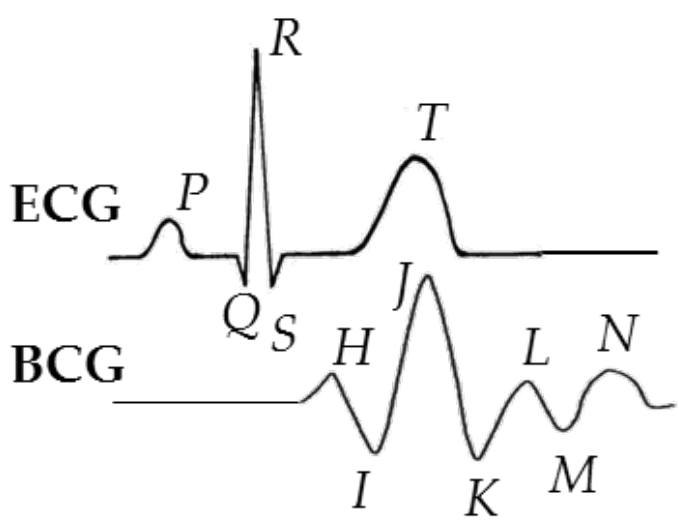


**Figure 2.** Typical ECG and BCG waveforms (18).

### 1.1.3. Respiration

When air is inhaled, the lungs expand and when it is exhaled, they contract. Respiration involves muscles that change the volume of the thoracic cavity to generate inspiration and expiration. During the flow of air into the lungs, the diaphragm moves downward and increases the lung volume. In addition, intercostal muscles surrounding the thoracic cavity move the rib cage in and out. Breathing depends upon cyclical respiratory muscle excitation by the motor nerves to the diaphragm and the intercostal muscles (30). Common respiratory measurements are usually performed by indirect methods. For example, nasal thermistors measure the temperature changes in the air and strain gauges positioned on the chest measure the changes in lung volume.

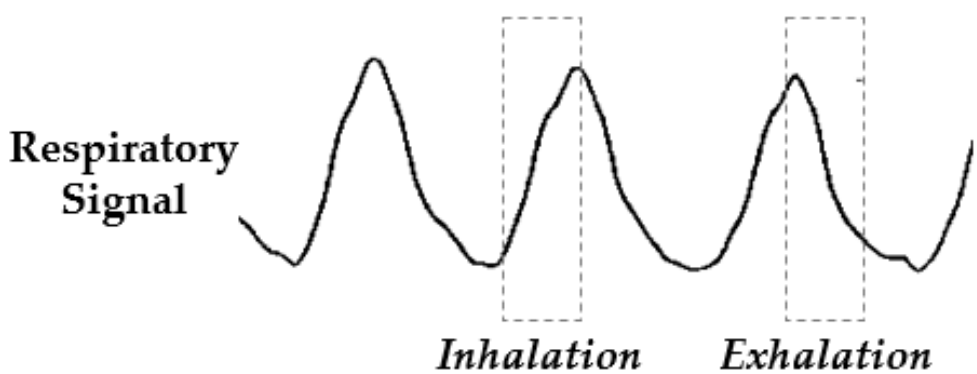


**Figure 3.** Typical waveforms of respiratory signal.

### 1.1.4. Heart rate and breathing rate

Heart rate (HR) is defined as the number of heart contractions per minute. Normally it varies within 60 – 100 beats per minute for healthy adults (60) and 70 – 170 for infants (28) in a resting state. It could become changed by provocation behaviors such as physical exercise, sleep, anxiety, stress, illness, and ingestion of drugs. Breathing rate (BR) is the number of breaths per minute in the process that moves air in and out of the lungs. The typical BR can vary from 12 to 16 breaths per minute for adults and 22 to 60 for infants. Usually, it is not completely regular and changes with exercise, fever, illness, and during talking (28,30,60).

### 1.1.5. Variability analysis of heart and respiratory rate

Variability analysis, the study of beat-to-beat (HR) or breath-to-breath (BR) interval fluctuations in cardiorespiratory information, has been applied to a number of physiological measurements, known as heart rate variability (HRV) and respiratory rate variability (RRV), respectively. Research has demonstrated that altered variability is present in association with pathological conditions and correlates with age, stress, illness, and disease. HRV became widely known for its ability to characterize autonomic nervous system (ANS) modulation of heart rate. This has prompted its application in the clinical setting to assessing a number of pathological conditions, including cardiovascular diseases, sepsis, diabetes mellitus, and trauma, as well as adverse events occurring during anesthesia. Furthermore, suppressed HRV has been correlated with disease severity and can serve as a predictor of morbidity and mortality. Similarly, RRV has been introduced recently in the clinical setting to monitor mechanically ventilated patients,

trauma patients, and pediatric patients (3).

## 1.2. Unobtrusive sensing methods for continuous physiological monitoring

Healthcare technology continues to evolve toward the objective of constructing a routine health management system. An essential requirement of such a system is continuous physiological signal monitoring (37). In the past, conventional methods of physiological measurement often caused discomfort by keeping subjects immovable or attaching various pieces of equipment to their bodies. However, these methods have been improved with the development of electronic technologies. Now, unobtrusive measurement technologies provide the possibility of managing subjects' health status as they go about their day-to-day lives (46).

Researchers have been actively developing technologies to detect biological information from individuals without confining them or causing any discomfort. The most commonly studied methods for unobtrusive sensing include capacitive, photoplethysmographic, ballistocardiographic, and seismocardiographic approaches (26,64).

The capacitive-coupled sensing method assumes the patient's skin and an electrode to be two layers of a capacitor, such that bio-potentials can be measured without any direct contact with the surface of the patient's body (38). Its application has been extended to unobtrusive wearable devices with measuring modules integrated or embedded into clothes or accessories (64). BCG measures the reaction forces of the body resulting from ventricular blood ejection, whereas a seismocardiogram (SCG) involves the measurement of the local fluctuations of the chest that are caused by a heartbeat. Wearable BCG and SCG units rely on attachable accelerometers

integrated into the support device (22,26). Photoplethysmogram (PPG) sensing devices use light-emitting diodes to illuminate the skin and photo-detectors to measure changes in light absorption. To achieve unobtrusive measurement, PPG measuring modules can be integrated into clothing, such as gloves or hats, or accessories, in the form of rings or ear-worn sensors (46, 47,64). Although there have been many different types of monitoring devices, Tamura *et al*. suggested that they can be roughly classified into three categories: portable, wearable, and invisible (Figure 4, 54).

These novel methods, which unobtrusively monitor the biological activity of subjects during their everyday life, can be used to set up a continuous examination system for long periods. They can also be used effectively for subjects who are difficult to confine physically, such as the elderly, infirm, and infants.


**Figure 4.** Examples of seamless monitoring of physiological information in daily life (54)

## 1.3. Outline of the dissertation

This dissertation contains the research approaches for developing an unobtrusive physiological signal monitoring system. We devised two unobtrusive sensing devices based on ECG and BCG measurements. They are described in detail with chapters divided into hardware and software sections.

- Chapter 2 contains the content about development of sensor devices for unobtrusive physiological signal measurement. First, BCG based physiological signal monitoring bed was designed for special use in health monitoring of infants. Fundamental experiments to validate the feasibility of the developed non-confining system based on load-cell sensors were conducted. Second, portable ECG monitoring patch was designed for pervasive health monitoring in daily life. To enhance the portability and wearability, the device was designed using an integrated minimized electrode array. Robustness of the device under motion was assessed by test protocols involving activities of daily life.

- Chapter 3 contains the content about development of algorithms for automatically analyzing unobtrusively measured signals. For the unobtrusively measured BCG signal analysis, an algorithm that includes an automatic sensor selection with a signal quality check function was developed to analyze the HR and BR accurately from the measured load-cell signals. For the

unobtrusively measured ECG signal analysis, a built-in algorithm that detects important ECG peaks was developed. Experiments were carried out to evaluate the performance of the developed algorithms. Software including an algorithm that analyses HRV was also developed and verified by a simulation study, assuming a condition in which some data was missing. Lastly, experiments were performed to assess the applicability under stressful conditions by using HRV analysis software.

- Chapter 4 and Chapter 5 summarize the results and present the conclusion. It is believed that the proposed devices and algorithms are essential for achieving pervasive health monitoring using unobtrusive sensors. This system can help users better understand their state of health and provide physicians with more reliable data for objective diagnosis.

This dissertation is based on the following publications. Thus, the main content of these publications is reproduced as a part of this dissertation.

I. Lee WK, Yoon H, Han C, Joo KM, Park KS. Physiological signal monitoring bed for infants based on load-cell sensors. *Sensors* 2016; 16: 409.

II. Lee WK, Yoon H, Park KS. Smart ECG monitoring patch with built-in R-peak detection for long-term HRV analysis. *Ann Biomed Eng* 2016; 44: 2292-301.

III. LEE WK, Yoon H, Jung DW, Hwang SH, Park KS. Ballistocardiogram of baby during sleep. Proceedings of 37th Annual International IEEE EMBS Conference; 2015; Aug 25-29; Milan, Italy. IEEE; c2015. p. 7167-70.

The author contributed to the publications as follows: conceived and designed the experiments, performed the experiments, analyzed the data, developed the analysis tools, and wrote and reviewed the manuscript.

*Chapter* **2**

# Development of sensor device for unobtrusive physiological signal measurement

## 2.1. Unobtrusive BCG measurement device for infants' health monitoring

Physiological signal monitoring could become pervasive in our daily life without causing any discomfort through the use of wearable device (clothes and accessories) or commonly used objects (furniture and tools). These novel methods, which unobtrusively monitor the biological activity of subjects during their everyday life, can be used to set up a continuous examination system for long periods. They can also be used effectively for subjects who are difficult to confine physically, such as the elderly, infirm, and infants. In particular, it is expected that unobtrusive biomonitoring for infants could play an important role in managing breathing and cardiovascular problems, which are the main causes of infants' death (1,42,59).

Conventional methods of physiological signal monitoring over long periods have limitations when applied to infants. For example, electrocardiography using adhesive electrodes can cause skin allergies or inflammation. In some cases, the skin can be seriously damaged when

detaching the electrodes from the body (11,59,62). In addition, respiratory measurements can cause discomfort and irritation, as the equipment must be fastened firmly to the body (1). Unobtrusive methods such as attaching a sensor to the nose (13) or foot (in the form of a sock) (17) have been used to measure biological information from infants. However, these methods still require the direct attachment of sensor devices to the body, which can be uncomfortable. Other indirect measuring methods include infrared thermography (1), piezoelectric force sensors (62), and Doppler radar (20). Further investigations related to the clinical verification of these approaches is ongoing.

Ballistocardiography represent a possible solution for monitoring infants' physiological signals. It is non-invasive instrument that measures the reactional motion of the body produced by cardiac contraction. Unlike electrocardiography, which require electrodes to be attached directly to the patient's body to detect electric signals, the ballistocardiography generally use sensors for force, pressure, vibration, and displacement. These sensors do not require direct attachments, and therefore, they allow the measurement of physiological signals for long periods of time without perturbing the subject (22,26). However, most studies investigating the application of these methods have focused on adults, and few cases have been focused on infants. More studies are necessary to verify the usefulness of BCG-based physiological measurement in infants. In a previous study, we developed a load-cell installed bed to measure the cardiac activity, respiration, and movement of adults (10,32). The basic concepts of the present system, including the load-cell's arrangement and the circuit design, are based on the former system. However, the detailed hardware specifications differ to account for relatively lightweight infant subjects.

Because it is more difficult to obtain complete BCG signals from their immature hearts, which have smaller cardiac output than adults (15).

Figure 5a illustrates the design of the physiological signal monitoring bed for infants proposed in this study. The size of the bed is 60 cm × 90 cm, and four load-cells (CBCL-6L, Curiosity Technology, Paju-si, Gyeonggi-do, Korea) are installed below the plane of the bed. The load-cell, which comprise four strain gauges in a Wheatstone bridge configuration, create an electrical signal in accordance with the force changes caused by cardiac activity and respiratory movements.

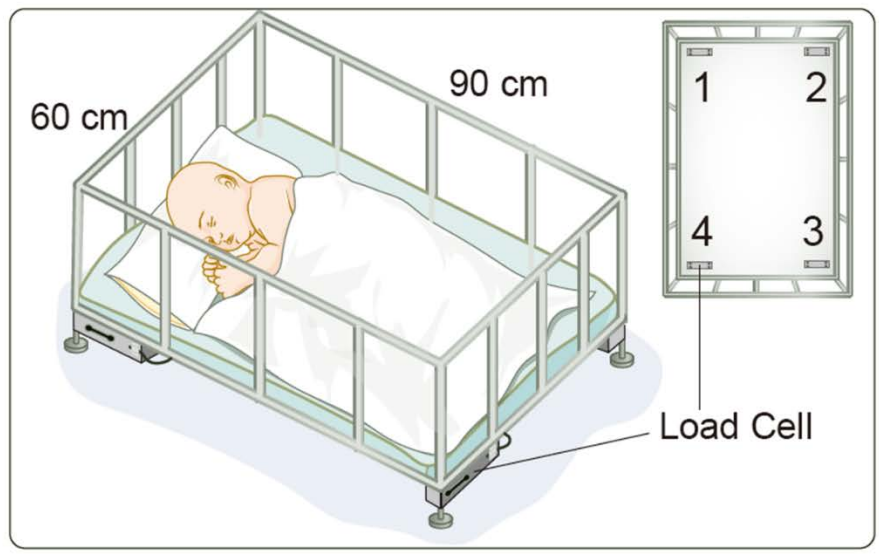


(a)

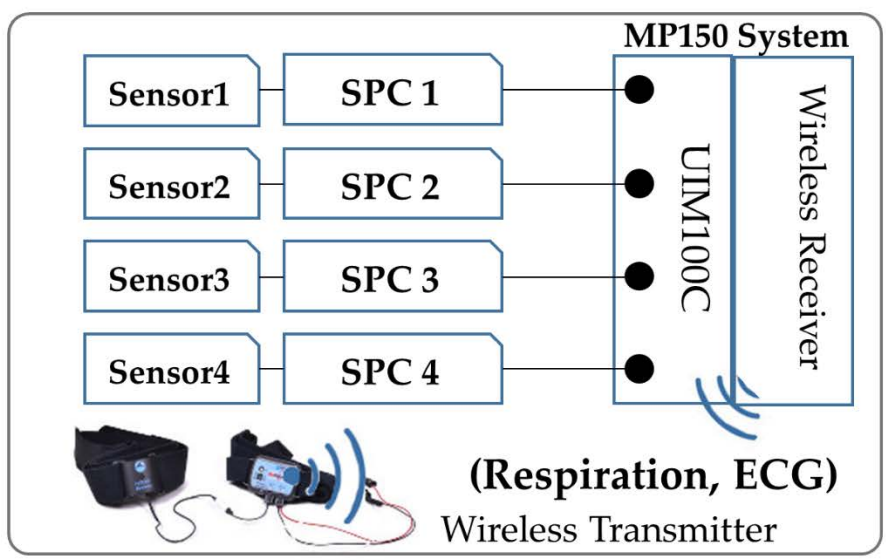


(b)

**Figure 5.** (a) Design of physiological signal monitoring bed for infants; (b) Experimental setup of signal acquisition system. (SPC: signal processing circuit)

### 2.1.1. Specifications of the device

The technical specifications of the load-cell sensor are provided in Table 1. A single point load-cell, a type of resistive load-cell, is generally used in the industry, and it features superior off-center loading compensation. The gage factor is defined as the ratio of the fractional change in the electrical resistance to the given strain, and it is typically around 2 for metallic strain gauges. Most manufacturers express the output of load-cell in units of mV/V, which is called the rated output. It is dependent on the gage factor and the operating stress of the load-cell structure, and it may range from 1 to 4 mV/V (a value of 2 mV/V is most common). For example, a load-cell with a rated output of 2 mV/V produces an output of 24 mV when supplied with excitation voltage of 12 V.

**Table 1**. Technical specifications of load-cell sensor

| **Single Point Load-Cell** |  |
|---|---|
| Load-cell material | Anodized Aluminum |
| Gage factor | 2.05 |
| Rated output | 2.0 ± 0.2 mV/V |
| Repeatability | 0.01 (% Rated output) |
| Creep | 0.03 (% Rated output, 30 min) |
| Zero balance | 0 ± 0.1 mV/V |
| Maximum excitation | 15 V (DC) |
| Maximum capacity | 6 kg |
| Input resistance | 400 ± 20 Ω |
| Output resistance | 350 ± 3.5 Ω |

The sensitivity should be calculated based on the output and capacity of the load-cell as follows.

$$\textbf{Sensitivity of load} - \textbf{cell}\ (\textbf{mV/kg}) = \frac{\boldsymbol{output}}{\boldsymbol{capacity}} = \frac{\boldsymbol{excitation\ voltage}\ (\boldsymbol{V}) \times \boldsymbol{rated\ output}\ (\boldsymbol{mV/V})}{\boldsymbol{capacity}\ (\boldsymbol{kg})} \quad (1)$$

In this study, each load-cell (CBCL-6L) with rated output of 2 mV/V and excitation voltage of 12 V shows sensitivity of 4 mV/kg.

### 2.1.2. Signal processing in hardware

Figure 6a illustrates the schematic diagram of the signal processing circuit for conditioning the load-cell output. Although the signals from load-cell sensors were amplified by the excitation voltage, the output caused by the cardiac activity and respiratory movements are not large enough to be displayed meaningfully. Thus, they were passed through an additional signal processing circuit. A precision instrumentation amplifier (AD8221, Analog Devices Inc., Norwood, MA, USA) with a gain setting of 100 was used in the circuit. This amplifier was associated with an alternating current (AC)-coupled circuit using an active integrator-based feedback network from the output to the reference terminal. This AC-coupled circuit improves the resolution of small AC signals by lowering the noise floor. Furthermore, OP1177, which forces the output of the AD8221 to 0 V at low frequencies, acts as a high-pass filter with a cut-off frequency of 0.1 Hz (please refer to the AD8221 datasheet). The signal output from the AD8221 was then passed through a low-pass filter to amplify the signal to the cardiorespiratory

frequency range and suppress noise signals. This low-pass filter was composed of a Sallen–Key 8$^{th}$-order Butterworth filter with a cut-off frequency of 20 Hz and a gain setting of 30. As a result, the overall circuit had a gain of 3000 and filtering bandwidth of 0.1 – 20 Hz. The simulation results of the frequency response of the signal processing circuit are shown in Figure 6b. Most of the signal acquisition methods described above follow the procedures described in the literature (23,52).

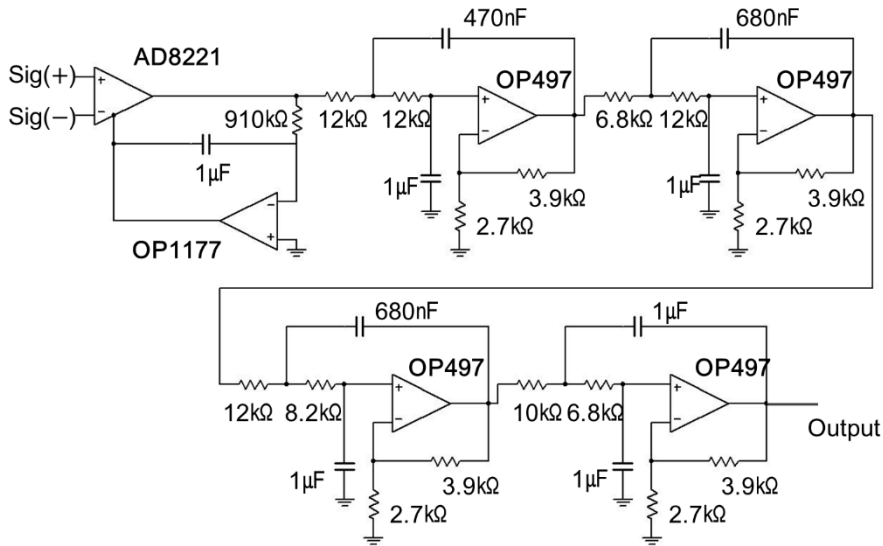


(a)

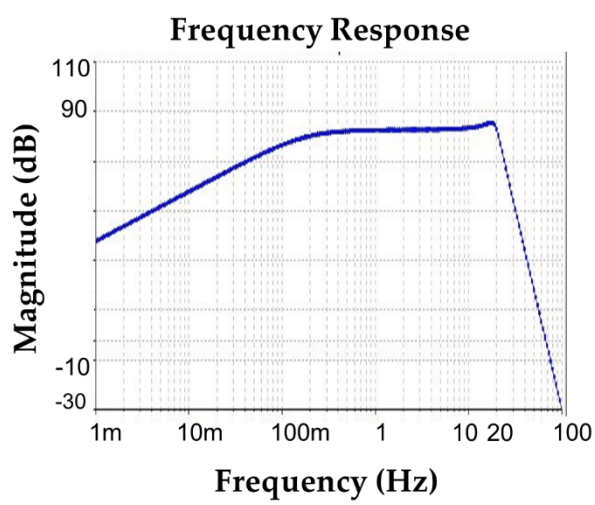


(b)

**Figure 6.** (a) Schematic diagram of signal processing circuit for the load-cell sensor; (b) Simulation results of frequency response of signal processing circuit.

### 2.1.3. Performance of the device

Although strain gauges, which consist of load-cell sensors, have a broadband dynamic response, mechanical platforms and their supports, with their large mass, behave as mechanical low-pass filters. Thus, it is important to check whether the overall frequency response of a load-cell integrated bed system can sense force components related to cardiac and respiratory activities (19).

The measuring setup shown in Figure 7 was configured for demonstrating the system's frequency response. The bed system was vibrated by an exciter (Modal Exciter Type 4824, Brüel & Kjær Sound & Vibration Measurement A/S, Nærum, Denmark) driven by a signal generator within the frequency range of 0 – 70 Hz. The details of the experiment followed procedures from the literature (14,19,24).

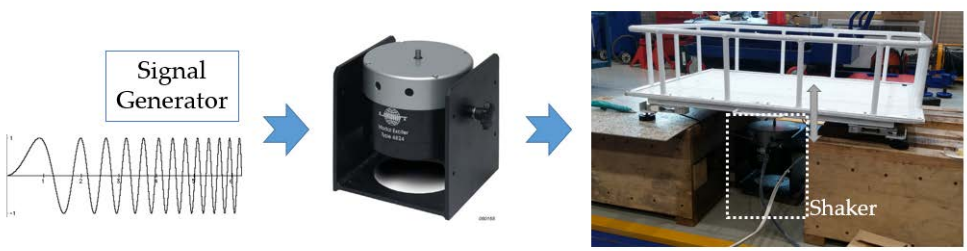


**Figure 7.** Setup for demonstrating the system's frequency response.

Figure 8 shows the results for resonant frequency of the load-cell integrated bed system. The resonant frequency was observed between 15 and 30 Hz for infants' body weights between 0 – 10 kg. According to Inan *et al.*, the "Majority of important information in BCG signals is contained below 10 Hz." (24)

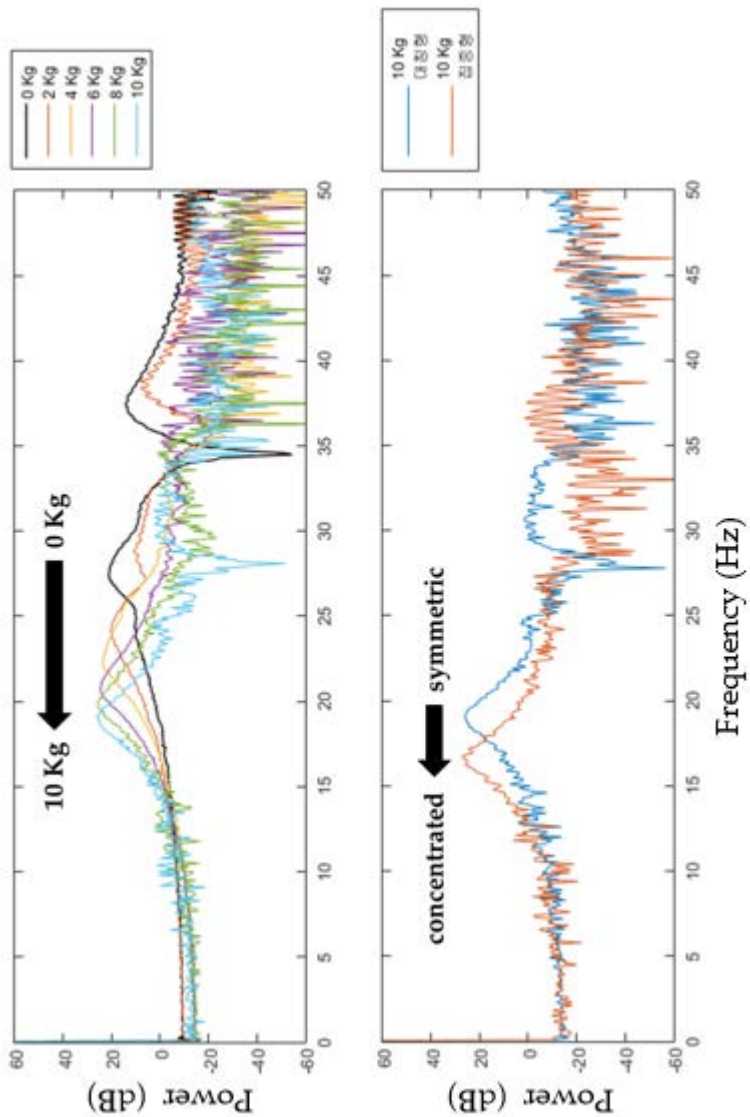


**Figure 8.** Results for resonant frequency of the load-cell integrated bed system.

Our experimental procedure limited the maximal load to 10 kg; however, this load is enough to demonstrate that the system has a resonant frequency higher than 10 Hz for monitoring an infants' physiological signal. In conclusion, our system is able to sense the force components related to cardiac and respiratory activities of infants.

Figure 9 shows a partial example of the monitored signals measured from a 19-month-old male subject, which is labeled as B-3. The output signals of the reference equipment (BN-RSPEC) are presented in (a) – (b), and the simultaneously acquired raw data from four load-cell sensors are presented in (c) – (f). Although the properties of the load-cell sensor outputs vary depending on a subject's lying position, most sensors can record both ballistic cardiac activities (localized rapid fluctuations) and respiratory movements (slow oscillations in sensors 2 and 3). A detailed analysis is presented below in the discussion section. Figure 9g shows a typical BCG waveform from the literature and also shows some of the characteristic peaks in comparison with the ECG signal. Most named waveform features in the BCG signal are clearly shown in the magnified view of our example of monitored signals (Figure 9h).

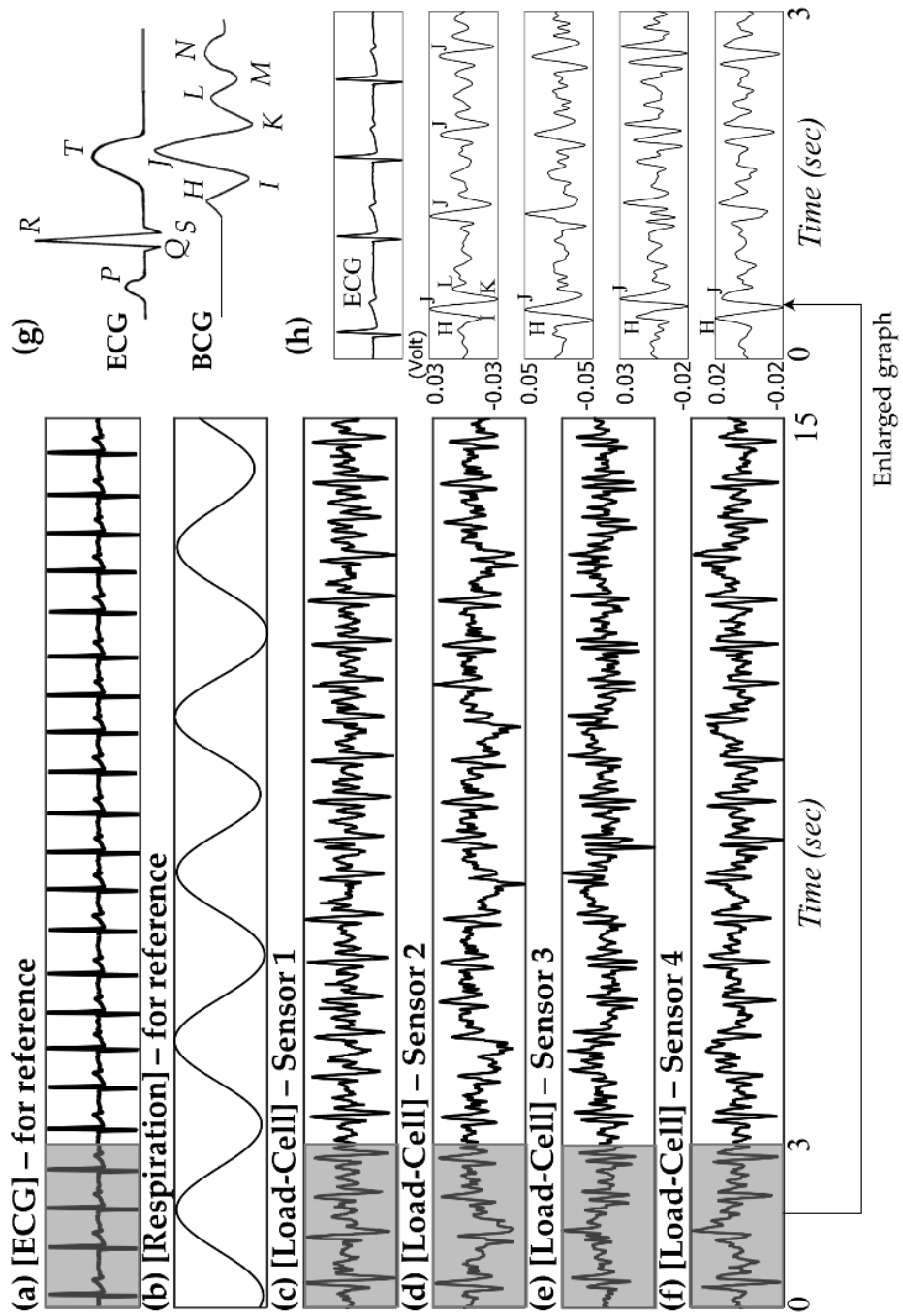


**Figure 9.** Simultaneous recordings of (a) ECG, (b) respiration signal, and (d) – (f) raw signals from four load-cell sensors, (g) typical BCG waveform (redrawn from literature (18)), and (h) waveform features of the BCG signal in our study.

## 2.2. Unobtrusive ECG measurement device for health monitoring in daily life

ECG monitoring is a typical form of U-healthcare. Electrocardiography records the electrical changes on the surface of the body by using the electric current that flows through the cardiac tissue. Clinically, it is most commonly used for diagnosing diseases related to cardiac activities and coronary vessels. Especially, HRV analysis, which continuously measures the variation in the heart rate, is used as a non-invasive physiological indicator that can predict the risk of cardiovascular diseases and quantitatively measure the balance between the sympathetic and parasympathetic nervous systems (34). The "standard limb leads" electrocardiographic method is commonly used in clinics. Although it can provide an accurate ECG that can be used for diagnosis, it requires the assistance of a specialist because of the cost, size, and weight of the equipment, and is thus inconvenient. Furthermore, cardiac disorders may not occur constantly but rather irregularly and sporadically. Therefore, there is a need for a convenient portable system that can continuously monitor the ECG and enable the management of the wearer's health status as he/she goes about his/her day-to-day life (36,61,64).

Various studies are being conducted to develop a technique that can satisfy these needs. The Holter monitor is one of the most commonly used ambulatory electrocardiography devices in the clinical field. In its early years, the device was large and heavy and usually caused discomfort to the patient, given that it required many electrodes be connected to their bodies, with wires. However, the device has since improved and now uses smaller recorders—although the size varies depending on the manufacturer—and uses relatively few leads, such that the patient remains comfortable during

recording (7,68). Other novel ECG monitoring devices that have been developed to provide portability include those which use only one or two leads (46) or devices based on capacitance-coupled sensing (31).

This study set out to design a new ECG monitoring system that integrates many of the advantages of the devices described above, based on recent studies, as well as the characteristics of various portable monitoring devices. We devised a small, lightweight ECG monitoring device that can be attached to the patient's torso. This device implements a modified lead arrangement, minimizing the distance between the electrodes required to measure the biologic signals. This allows all the electrodes to be on a single patch, which is easy to attach and detach to and from the measuring device by using a snap button. We also compared the results obtained with our device with those obtained with a commercial device for common day-to-day activities such as laying down, sitting, and walking.

### 2.2.1. Specifications of the device

We developed a portable ECG monitoring device that can easily measure the ECG by connecting the measuring module to a patch with a minimized electrode array using a snap button. The measuring module, which is illustrated in Figure 10a, is small (38 mm wide, 38 mm long, and 7 mm thick), such that it can be held in the palm of one's hand. The weight of the module, including the battery, is 10 g.

Considering the minimum required potential difference, the electrodes were arrayed over a patch (patch electrode), which is illustrated in Figure 10b, with a width of 150 mm and a length of 60 mm, weighing 4 g. The material used for the patch is non-woven fabric with hydrogel and

adhesive. We verified the biocompatibility of the two components (hydrogel, adhesive) that are in contact with the skin and they were found to have passed all the test requirements including cytotoxicity and skin irritation as proposed by the FDA and ISO 10993-1 for materials to be in contact with uncompromised skin. An Ag/AgCl-based electrode array is printed into the patch and protected by an insulation coating. As a result of the effect of the insulation coating, the patch electrode exhibits a uniform impedance and stable performance even when subjected to sweat and moisture.

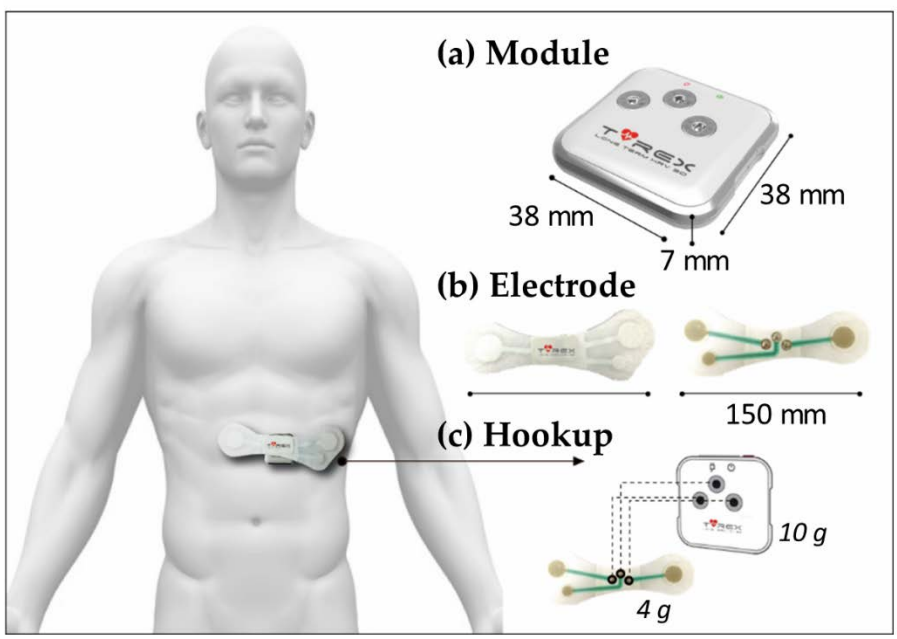


**Figure 10.** Smart ECG monitoring device.

Attaching and detaching the patch to and from the measuring module by using a snap button (as illustrated in Figure 10c) not only reduces the burden of attaching multiple lead electrodes to the body, but also reduces the noise emanating from the cables, allowing the measurement of more stable signals. When using the device, the user connects the measuring

module to the patch electrode, attaches it to his or her torso (near the celiac plexus), and then presses the power button for about two seconds. A blue LED blinks to indicate whether the ECG signals are being detected normally. Because it is highly portable, convenient, and easy to use, ECG monitoring is possible at any time of the day or night, even while the subject is asleep. The equipment uses a 3.7 V lithium polymer battery as its power source, which enables it to operate for around 90 h when fully charged. To enable longer monitoring, the equipment maximizes its use of the limited energy in the battery by entering energy-saving mode (disabling the peripherals) when the system is not operating.

### 2.2.2. Signal processing in hardware

The measuring module is composed of amplifying and filtering circuits which can detect ECG signals from the leads attached to the wearer's body, an accelerometer for detecting movement and the body's posture, and a processor that performs functions such as signal processing and data transmission. An instrumentation amplifier (AD8235, Analog Devices Inc., Norwood, MA, USA), which has a high common-mode rejection ratio (CMRR = 100 dB) was used to amplify only the differential of the obtained signal. In addition, in an attempt to reduce the effect of noise and improve the R peaks of the ECG, we designed band-pass (5.9 to 48 Hz) and notch (60 Hz) filtering circuits by using quad op amps (LT6005, Linear Technology, Milpitas, CA, USA) with a CMRR of 100 dB. The acceleration transducer was configured using a digital output motion sensor with a 3-axis acceleration indicator (LIS3DH, ST Microelectronics, Geneva, Switzerland).

We used a microcontroller (STM32F103, STMicroelectronics) with a

Cortex-M3 core, to build the main processor. The main control unit, operating at a 72 MHz clock speed, not only includes a variety of peripheral devices such as 512 KB of flash memory, 64 KB of SRAM, and a 12-bit analog to digital converter, but also supports communication interfaces such as a serial peripheral interface (SPI), universal serial bus (USB), and universal asynchronous receiver & transmitter (UART). To enable the connection of the measuring equipment to the computer, the data transfer part conforms to the communication device class (CDC) of the USB interface; a diagram of the device is shown in Figure 11.

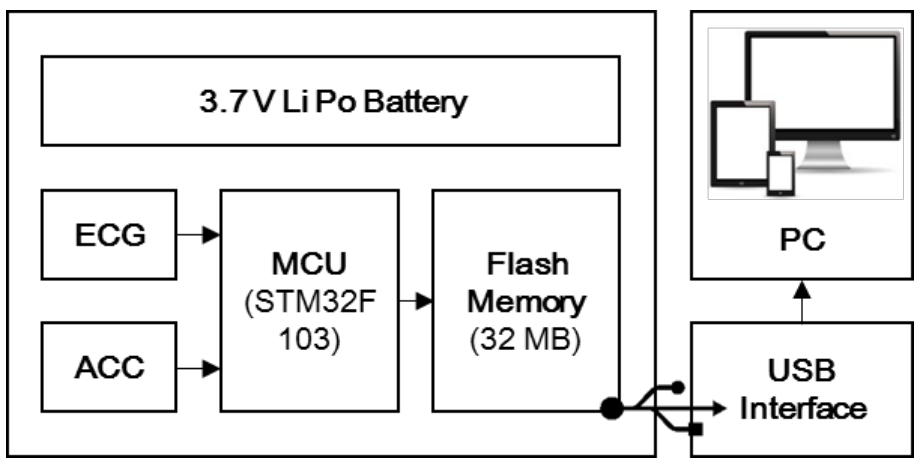


**Figure 11.** Architecture of developed device.

Our device supports the collection of an ECG signal with a 12 bit resolution and a 256 Hz sampling frequency, as well as an acceleration signal with a 16 bit resolution and 1 Hz sampling frequency. The collected data is saved to a 32 MB serial flash memory block, from which the ECG and acceleration signal for the last 24 hours can be reviewed (the reviewable duration can be extended by increasing the capacity of the memory up to 128 MB). Since the ECG signals of each individual have different amplitudes, the

equipment automatically examines the waveform of the ECG saved in the memory and controls the gain of the amplifier to amplify the ECG signal to attain a consistent amplitude.

### 2.2.3. Performance of the device

We set out to compare and evaluate the ECG data obtained using both a commercial device and the newly developed device. For this comparison, we planned to validate the accuracy of the new ECG device when applied to day-to-day activities. Twelve adult males and females (average age 26.8 (± 3.1)) without any history of cardiovascular disorders enrolled in this study. Lying in bed, sitting on a chair, and walking were selected as day-to-day activities. After attaching an ECG monitoring patch to a subject's torso, the ECG was measured while he/she laid in bed for 10 min, sat on a chair for 10 min, and walked on a treadmill at a speed of 1, 3, and 5 km/h, respectively, for 5 min. The total ECG data duration was 35 min per subject.

To compare the data obtained with the developed device with that obtained with a conventional device, another ECG was obtained simultaneously using a data-acquisition system (MP150, BIOPAC System, Inc., Goleta, CA, USA) with a sampling rate of 1000 Hz. Commercial devices utilize Ag/AgCl electrodes to detect ECG signals in the Lead-II position. The electrodes are connected to the measuring devices using wires. Wires are attached to the body with tape to reduce the noise generated by movement. In a conventional Holter system, the Holter device is fixed to the waist, with the wires connected to the machine and the electrodes attached to the body with tape. We mimicked this wire/device array.

In addition to evaluating the quality of the signals according to the

amount of noise, the estimated signal-to-noise ratios (SNRs) of the ECG signals obtained simultaneously from both the commercial and developed devices were compared. The details of the SNR estimation were conducted following procedures from literature (25,63). This estimation methodology accounts for all sources of noise and interference that affect the signal quality, including electronic noise and motion artifacts (27). The R-peak detection and SNR calculation were done using software (MATLAB R2014b, The Math Works, Inc., USA).

We measured the ECG using a conventional device and our device, in conditions representing day-to-day activities (*i.e.*, lying position, sitting position, and walking at 1, 3, and 5 km/h). A total of 120 sets of ECG data were obtained (60 from the conventional device, 60 from our device). The quality of the signals was assessed according to the amount of noise estimated by the SNR methods. Figure 12a shows a comparison of the mean SNR estimation of our device to a conventional device for this experiment. The values of the SNR analysis for the two data sets show similar results for small-movement conditions such as lying and sitting. However, for a walking speed of 1 km/h or more, a considerable amount of noise arose. Thus, there is a significant difference between the SNRs of the results obtained with the two devices. Our device, which is superior in terms of signal quality, shows a high SNR. Figure 12b and Figure 12c are a box-plot comparison of the SNRs and a frequency distribution table of the SNRs, respectively. Among these, the 5 km/h data for subjects 4, 6, 10, and 12 were compared and shown in Figure 13.

.

| | Lying | Sitting | 1 km/h | 3 km/h | 5 km/h |
|---|---|---|---|---|---|
| Commercial | 21.79±1.23 | 19.91±1.40 | 13.94±4.28 | 8.46±6.89 | 5.64±6.53 |
| Developed | 20.19±1.80 | 18.76±1.91 | 18.00±2.63 | 14.99±4.90 | 12.76±6.13 |

(a)



(b)

| SNR (dB) | Com-mercial | Deve-loped |
|---|---|---|
| 10 < SNR | 43 | 55 |
| 5 < SNR ≤10 | 9 | 2 |
| 0 < SNR ≤ 5 | 2 | 3 |
| -5 < SNR ≤ 0 | 5 | 0 |
| SNR ≤ -5 | 1 | 0 |

(c)

**Figure 12.** Comparison of SNR between commercial and developed devices under conditions representing daily activities: (a) mean data, (b) box-plot comparison, (c) frequency distribution table.

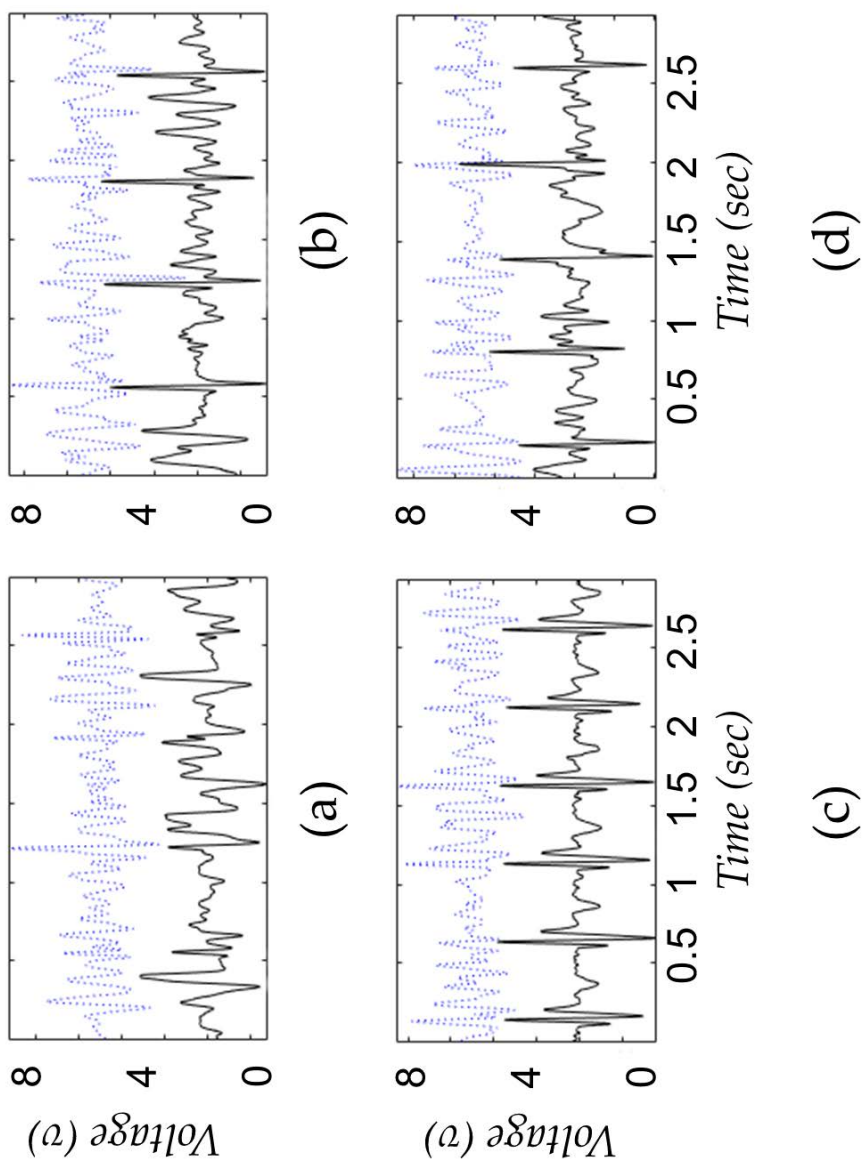


**Figure 13.** Examples of ECG signals recorded using a commercial device (blue dotted line) and the developed device (black line): 5 km/h data for (a) subject 4, (b) subject 6, (c) subject 10, (d) subject 12.

# Chapter 3

# Development of algorithm for physiological information analysis from unobtrusively measured signal

## 3.1. Algorithm for automatically analyzing unobtrusively measured BCG signal

We propose a non-confining system for monitoring the biological information of infants using ballistocardiography technology in Chapter 2.1. In addition, an algorithm that includes an automatic sensor selection with a signal quality check function has been developed to analyze the heart rate (HR) and breathing rate (BR) accurately from the four measured load-cell signals. The final objective is to validate and evaluate the feasibility of the infant biological information monitoring system. In experiments on infant subjects, the designed bed was used to acquire biological data, and the biological information from the proposed algorithm was compared with the reference information obtained simultaneously.

### 3.1.1. Process flow of the algorithm

We designed an algorithm that performs automatic sensor selection with a signal quality check function to automatically analyze HR and BR. This algorithm consists of three stages: *pre-processing*, *signal quality check and sensor selection*, and *peak finding and calculation*. The basic concept of the proposed method is to iteratively shift a short analysis window across the signal. Although the overall flow applies equally to both heartbeat and respiration signal analysis, some details concerning the window length, pre-processing method, and criterion for artifact determination differ depending on the analysis objective. Figure 14 shows a flowchart outlining the algorithm used to estimate the HR and BR. The algorithm was independently operated for heartbeat and respiration signals (*i.e.*, there are two separate algorithms).

**Figure 14.** Flowchart of the proposed algorithms for automatic (a) HR and (b) BR analysis.

#### 3.1.1.1. Pre-processing of the data

Consider the original signals obtained from the proposed system, $\boldsymbol{x_k[n]}$ ($\mathbf{k = 1, \cdots, 4}$, the number of load-cell sensors), where $\boldsymbol{n}$ is the length of the analysis window. For the HR and BR analysis, we set $\boldsymbol{n}$ to 5 s and 30 s, respectively. Considering a sampling rate of 1000 Hz, 5000 samples were included in each HR analysis window, and 30,000 samples were included in each BR analysis window. In the general case, the signal $\boldsymbol{x_k[n]}$ includes components of cardiac activity (usually called BCG) and respiratory movement. The pre-processing stage applies an infinite impulse response (IIR) digital filter to extract the appropriate physiological rhythm, and it employs other signal processing techniques to enhance the peak component and suppress noise. To avoid any time delay or phase shift, zero-phase digital filtering (offered by the "filtfilt" function in the MATLAB software) was applied in all the following filtering processes. Zero-phase digital filtering, which was conducted by processing the input data in both the forward and the reverse directions, reduces noise in the signal and preserves the peak at the same time at which it occurs in the original.

**• Pre-processing for the HR analysis**

The signal is first separated using a fifth-order band-pass Butterworth filter (IIR) with a range of 1 – 20 Hz to extract clear heartbeat derived signals (Figure 15b, denoted as $\boldsymbol{f_{HR}(x_k[n])}$ ). Subsequently, first-order differentiation is applied to the signals $\boldsymbol{f_{HR}(x_k[n])}$ to extract information about the slope and accentuate the main peak component (Figure 15c, denoted as $\boldsymbol{dBCG_k[n]}$). The $\boldsymbol{dBCG_k[n]}$ signals are implemented as

$$\boldsymbol{dBCG_k[n] = f_{HR}(x_k[n+1]) - f_{HR}(x_k[n])}. \quad (2)$$

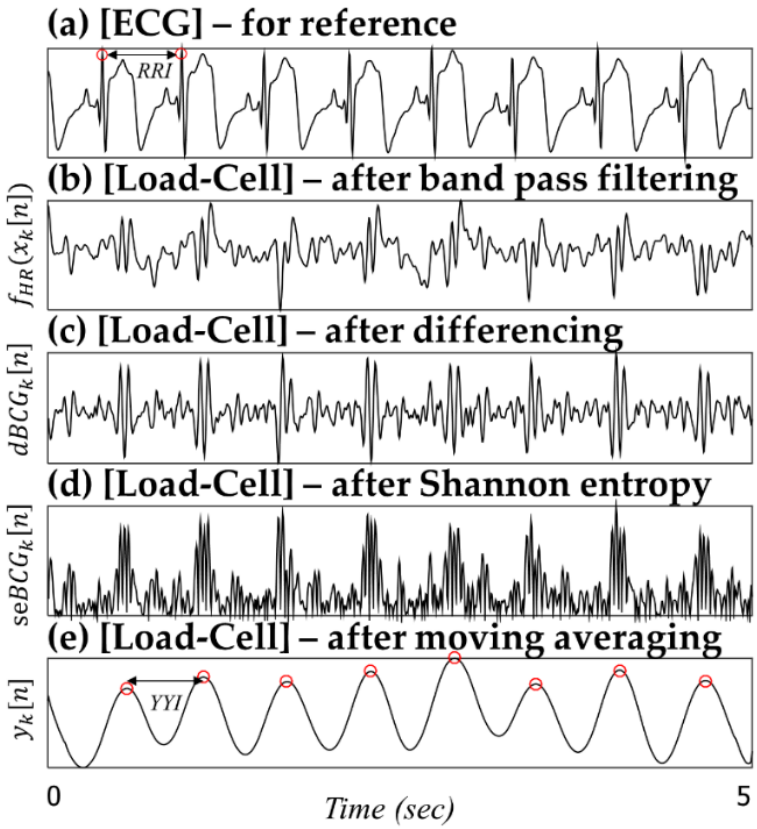


**Figure 15.** Pre-processing steps for the HR analysis.

The differentiated signal ($\boldsymbol{dBCG_k[n]}$) is passed through a nonlinear transformation to obtain positive peaks regardless of the polarity of the main peak components (Figure 15d, denoted as $\boldsymbol{seBCG_k[n]}$). The main objective of this transformation is to enhance the main peak components and use a single-sided threshold mechanism. The nonlinear transformation giving the Shannon entropy value is applied as follows:

$$\boldsymbol{seBCG_k[n] = -|dBCG_k[n]| \times \log(|dBCG_k[n]|)}. \quad (3)$$

Finally, a moving average filter is applied to smooth out the spikes and noise bursts (Figure 15e, denoted as $\boldsymbol{y_k[n]}$). The signal quality check and

sensor selection stage then determine the optimum signal, and the corresponding $\boldsymbol{y_k[n]}$ signal is passed to the peak finding and calculation stages.

In Figure 15, for example, according to the seven successive RR intervals (intervals between the R-peaks from the ECG signal), the average RR interval (RRI) from the ECG signal is 0.5874 ± 0.0169 s. In contrast, the average YY interval (YYI) from the $\boldsymbol{y_k[n]}$ signal is 0.5851 ± 0.0226 s. Additionally, the average difference between RRI and YYI (|RRI-YYI|) is 0.0103 ± 0.0069 s. Heartbeat information can be extracted quite well by applying the above data processing stage. This preconditioning is useful for handling BCG signals with less-dominant peak components caused by small heartbeat amplitudes.

**• Pre-processing for the BR analysis**

For the BR analysis, the raw signals $\boldsymbol{x_k[n]}$ are first discerned using a fifth-order 0.5 Hz low-pass Butterworth filter (IIR) to extract the main respiratory rhythm (Figure 16c, denoted as $\boldsymbol{f_{BR}(x_k[n])}$). Although the original signals obtained from the developed system ($\boldsymbol{x_k[n]}$) have already passed through the electronic high-pass filter (AC-coupled circuit, fc = 0.1 Hz), some remaining low-frequency components can cause the baseline to wander. To suppress unwanted residual baseline drift, a de-trending technique based on empirical mode decomposition (EMD) is used to preprocess the signal $\boldsymbol{f_{BR}(x_k[n])}$ (16).

Hereafter, the de-trended $\boldsymbol{f_{BR}(x_k[n])}$ signal is denoted as $\boldsymbol{z_k[n]}$. As in the HR analysis, the peak finding and calculation stage are conducted according to the $\boldsymbol{z_k[n]}$ signal corresponding to the optimum signals selected by the signal quality check and sensor selection stages. In Figure 16,

for example, according to the 13 successive breathing intervals (BRI), the average breathing interval from the respiratory signal is 2.0945 ± 0.1354 s. In contrast, the average ZZI from the $\boldsymbol{z_k[n]}$ signal is 2.1015 ± 0.0945 s. The average difference between BRI and ZZI (|BRI-ZZI|) is 0.0545 ± 0.0349 s.

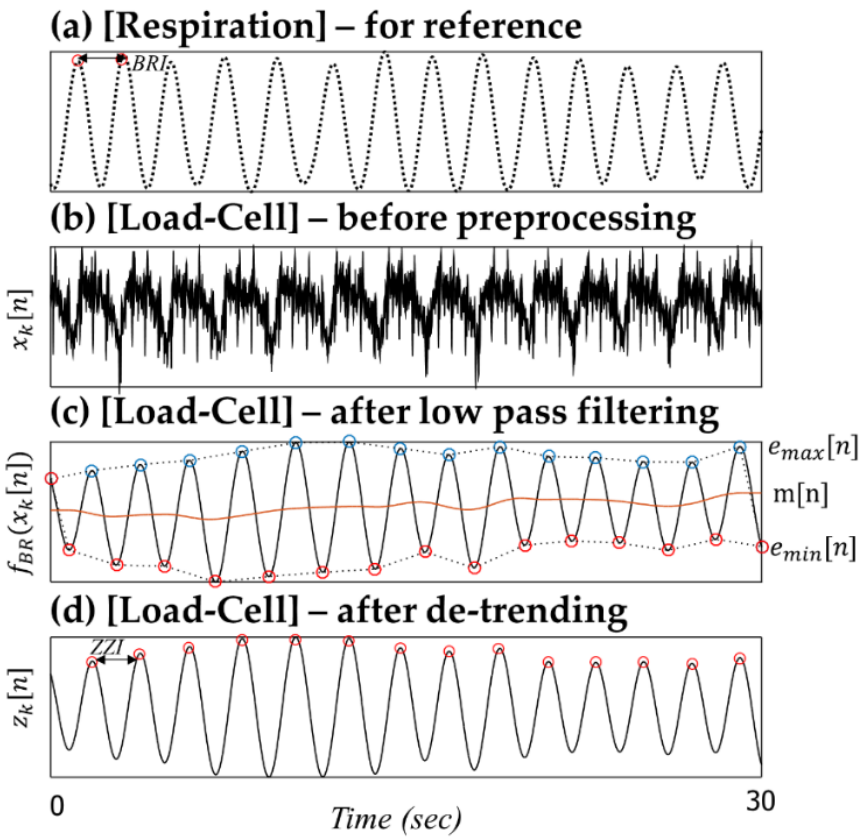


**Figure 16.** Pre-processing steps for the BR analysis.

#### 3.1.1.2. Signal quality check and sensor selection

The most important aspect of the signal analysis obtained from unobtrusive sensors is the signal quality. In particular, the signals obtained from the developed load-cell-based system are much weaker than other types of body signals. Therefore, it is important to separate that portion of the signal that includes useful biological information from the artifact component.

If the obtained signal is clearly recorded without artifacts, it can be assumed to exhibit special periodicity according to the heartbeat or respiratory cycles. Thus, the main objective of this stage is to determine whether the signal contains periodicity in the expected frequency region. The expected frequency region is set differently for HR and BR analysis. Let $\boldsymbol{f_l}$ and $\boldsymbol{f_h}$ represent the lower and higher frequencies of the expected frequency region. For HR analysis, these parameters were set to 0.8 and 2 Hz, respectively, whereas for the BR analysis, they were set to 0.2 and 0.8 Hz, respectively.

In addition, we developed signal quality indicators (THV-$S_k$) by using the calculated threshold parameters based on the autocorrelation (THV-$A_k$) and power spectral densities (THV-$P_k$). The indicators were used for estimating the level of artifacts in the following signal quality check and sensor selection processes. The following details of signal quality calculations for optimal sensor selection are illustrated in Figure 17 (HR) and Figure 18 (BR).

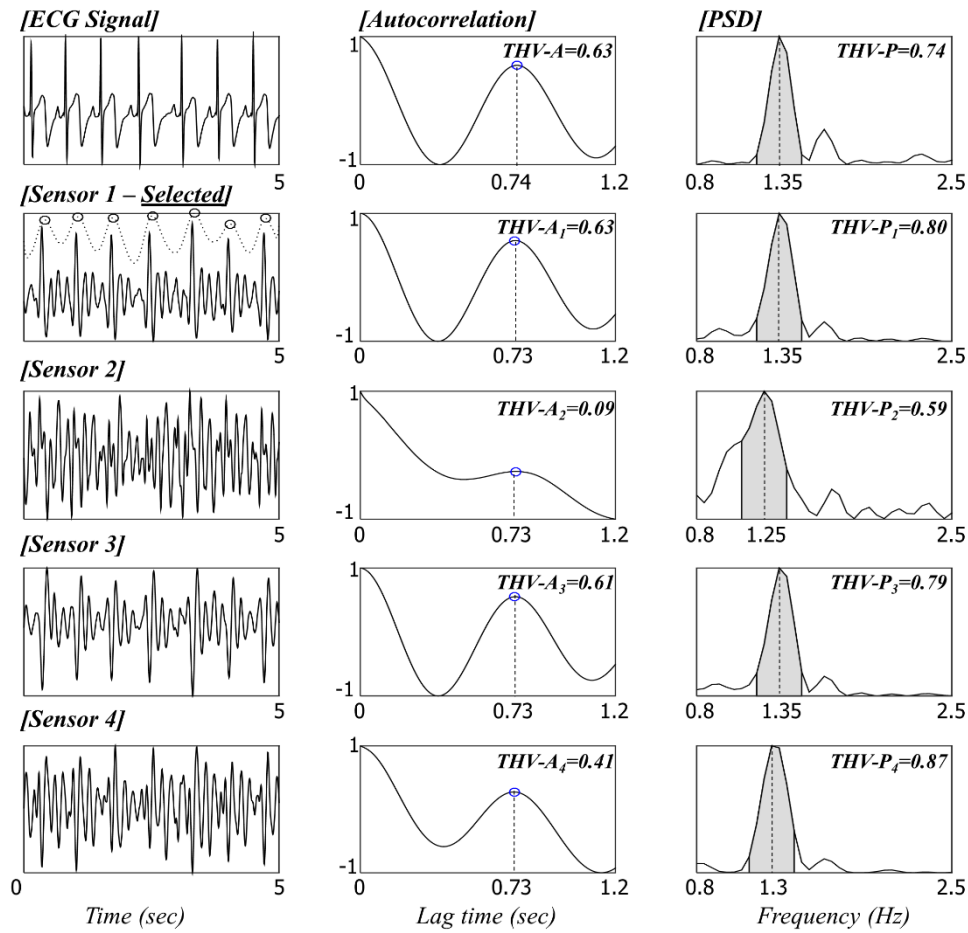


**Figure 17.** Signal quality check based on the THV-S and sensor selection for HR analysis.

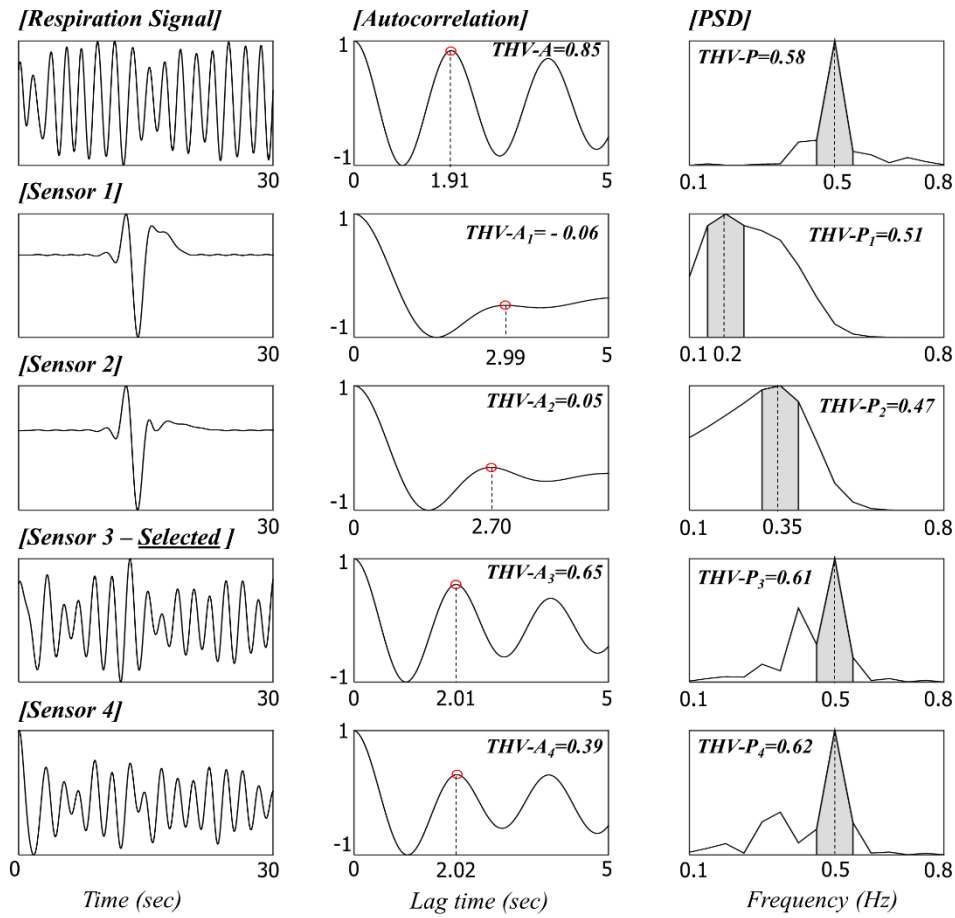


**Figure 18.** Signal quality check based on the THV-S and sensor selection for BR analysis (There are motion artifacts in the signals from sensors 1 and 2, and they were eventually excluded in the following sensor selection by the lower THV-S).

**• Autocorrelation-based threshold**

The autocorrelation function (ACF) measures the correlation between $\boldsymbol{b_t}$ and $\boldsymbol{b_{t+i}}$, where $\mathbf{i} = \mathbf{0}, \cdots, \mathbf{j}$. The autocorrelation formula ($\boldsymbol{r_j}$) for lag $\mathbf{j}$ is

$$\boldsymbol{r_j = c_j / c_0} \tag{4}$$

where $\boldsymbol{c_j = \frac{1}{T-1} \sum_{t=1}^{T-j} (b_t - \bar{b})(b_{t+j} - \bar{b})}$, $\boldsymbol{c_0}$ is the sample variance of the time series, and $\mathbf{T}$ is the total number of samples in the window for the ACF calculation. The lag $\mathbf{j}$ is determined using the lower expected frequency region explained above. For the HR and BR analysis, $\mathbf{j}$ was set to 1.25 s (= 0.8 Hz) and 5 s (= 0.2 Hz), respectively.

If the signal is clean and contains the periodicity of the heartbeat and respiratory cycles, peaks appear in the ACF graph (when the first derivative of ACF goes from positive to negative). In the case of multiple peaks, only the first is considered to represent the periodicity. When the position of the peak in the ACF is in the predetermined range of 0.5 – 1.25 s lag for HR and 1.25 – 5 s lag for BR, the algorithm regards the position to be normal. The ACF value at that peak is recorded as THV-$A_k$. If there is no peak in the range, THV-$A_k$ is set to 0. Such signals are often determined as being artifacts in the following signal quality check stage.

**• Power spectral density (PSD)-based threshold**

The PSDs of data within a short analysis window are calculated by a fast Fourier transform (FFT) method. We use a periodogram containing 20,000 discrete Fourier transform (DFT) points, which gives a spectral resolution of 0.05 Hz. The PSD-based threshold THV-$P_k$ is defined as the concentration ratio of the power summation. First, the maximum PSD in the expected

frequency region, between $f_l$ and $f_h$, is detected. If the frequency with the maximum power is denoted as $f_{max}$, then THV-$P_k$ is computed as

$$\text{THV-}P_k = \sum_{f=f_{max}-0.1}^{f_{max}+0.1} P_f / \sum_{f=0.1}^{f_h} P_f. \quad (5)$$

**• Signal quality check and selection of optimum sensor channel**

The signal quality check is conducted based on THV-$S_k$ (THV-$S_k$ = THV-$A_k$ + THV-$P_k$). If THV-$S_k$ is larger than the predetermined values of $THV_{HR}$ and $THV_{BR}$, the signal included in the current short window (of length 5 or 30 s for HR or BR, respectively) is considered to be clean. In this study, $THV_{HR}$ and $THV_{BR}$ were empirically set to 0.65 and 1.25, respectively.

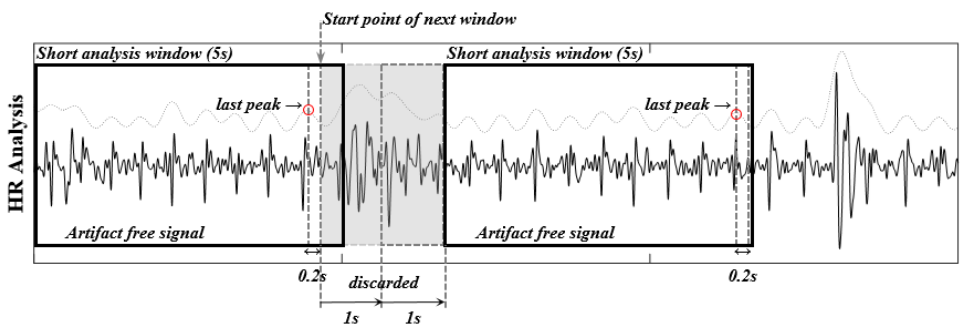


**Figure 19. Partial example of operating algorithm in HR analysis.**

If all THV-$S_k$ values are lower than the predetermined threshold, the signal in the current short window is considered to be an artifact. The short analysis window then slides along for 1 s until a clean signal is detected (*i.e.*, start point of window changes from $a_1$ to $a_1$ + 1 s). If more than one THV-$S_k$ value from the four load-cell sensors is higher than the predetermined threshold value, the sensor with the maximum THV-$S_k$ value is selected as the most suitable sensor for measuring the cardiac activity or respiratory

movement. Then, the peak included in the current short window of the most suitable sensor is detected, and the intervals between peaks are calculated. The short analysis window then jumps to the next start point. To prevent the case in which the peak may be located at the edge of the window, the next start point was set by considering the location of the last peak in the current window (for example, location of last peak + 0.2 s, as also shown in Figure 19).

### 3.1.2. Performance evaluation

#### 3.1.2.1. Subjects and experimental method

According to the Infant Care Act of Korea, preschool children under the age of six are considered infants. Four infants aged between 5 and 42 months (at the time of first participation) participated in the experiment after informed consent was received from their parents. Table 2 presents the physical characteristics of the four infants (labeled A through D) and experimental time. Because each subject participated more than once on different dates, a total of 13 experiments were conducted. The different dates for the same subject are indicated as, for example, B-1, B-2, and B-3. The experimental time shows somewhat irregular lengths. This was unavoidable because our experiments have some limitations related to the time constraints in accordance with the experimental conditions faced in home visits. Moreover, the subjects sometimes awoke easily when they were not in their own familiar bed. We have done our best to collect data for as long as possible. The experiment was approved by the Ethical Committee of Seoul National University Hospitals (IRB No. 1511-070-719).

**Table 2.** Physical information about the participating subjects and experimental time.

| Records | Gender | Age (Months) | Height (cm) | Weight (kg) | Experimental Time (min) | Data Length * (Sample) |
|---|---|---|---|---|---|---|
| A-1 | Female | 42 | 97.5 | 14.5 | 12 | 720,000 |
| A-2 | | 43 | 97.8 | 15.0 | 20 | 1,200,000 |
| A-3 | | 44 | 98.0 | 15.2 | 25 | 1,500,000 |
| A-4 | | 46 | 98.5 | 15.5 | 30 | 1,800,000 |
| A-5 | | 48 | 99.2 | 15.9 | 30 | 1,800,000 |
| B-1 | Male | 13 | 78.0 | 13.0 | 10 | 600,000 |
| B-2 | | 14 | 78.5 | 13.3 | 20 | 1,200,000 |
| B-3 | | 19 | 80.1 | 14.8 | 90 | 5,400,000 |
| C-1 | Male | 09 | 71.0 | 9.20 | 11.9 | 714,000 |
| C-2 | | 09 | 71.0 | 9.20 | 178.8 | 10,728,000 |
| C-3 | | 10 | 72.0 | 9.40 | 30 | 1,800,000 |
| C-4 | | 13 | 77.0 | 10.0 | 72 | 4,320,000 |
| D-1 | Male | 05 | 67.0 | 9.20 | 33 | 1,980,000 |

*: Data were collected at a sampling rate of 1000 Hz.

During each experiment, the infant was laid down and allowed to fall asleep on the monitoring bed. As references to validate the performance of the developed bed and algorithm for analyzing the HR and BR, the signals from an ECG electrode and a breathing sensor (BN-RSPEC, BIOPAC Systems, Inc., Goleta, CA, USA) were recorded. ECG and breathing signals were transmitted wirelessly to the data acquisition system (MP150, BIOPAC Systems, Inc., Goleta, CA, USA) by using a receiver, and the four output signals of the developed system were also recorded simultaneously by the same data acquisition system (MP150 with UIM100C module). The MP150 system internally has a single ground connection and a microprocessor to control the data acquisition and communication with the computer. The wireless system has a separate ground for each transmitter. All data were collected at a sampling rate of 1000 Hz (Figure 5b).

To evaluate the performance of the developed algorithm, the peak information from both the ECG and the respiratory signals (from the chest belt sensors) were labeled by researchers. An internally developed MATLAB-based software tool featuring automatic peak detection, manual peak marking, and correction was used in this peak annotation process. Information about the peak locations and derived intervals between peaks were used as a standard reference in the following performance evaluation.

First, the reliability of the proposed algorithm with respect to the beat locations was assessed using the following quantitative indexes. For the heartbeat location, we defined the beat location evaluation area that ranges from R peak location −0.15 s to R peak location +0.35 s. The beat location evaluation area considered the different peak timings derived from a dissimilar signal source, ECG (electrical signal), and BCG (mechanical signal). If the closest load-cell-derived heartbeat was within this beat location evaluation area, it was denoted as a true positive (TP), *i.e.*, it was correctly detected by the proposed algorithm. Other unassigned load-cell-derived heartbeats were counted as false positives (FPs). When no heartbeats were within the beat location evaluation area corresponding to an R peak in the ECG, it was counted as a false negative (FN). This process was similarly applied to the load-cell-derived respiratory signals. However, the beat location evaluation area for BR analysis was set to range from respiratory peak location −0.45 s to respiratory peak location +1.05 s.

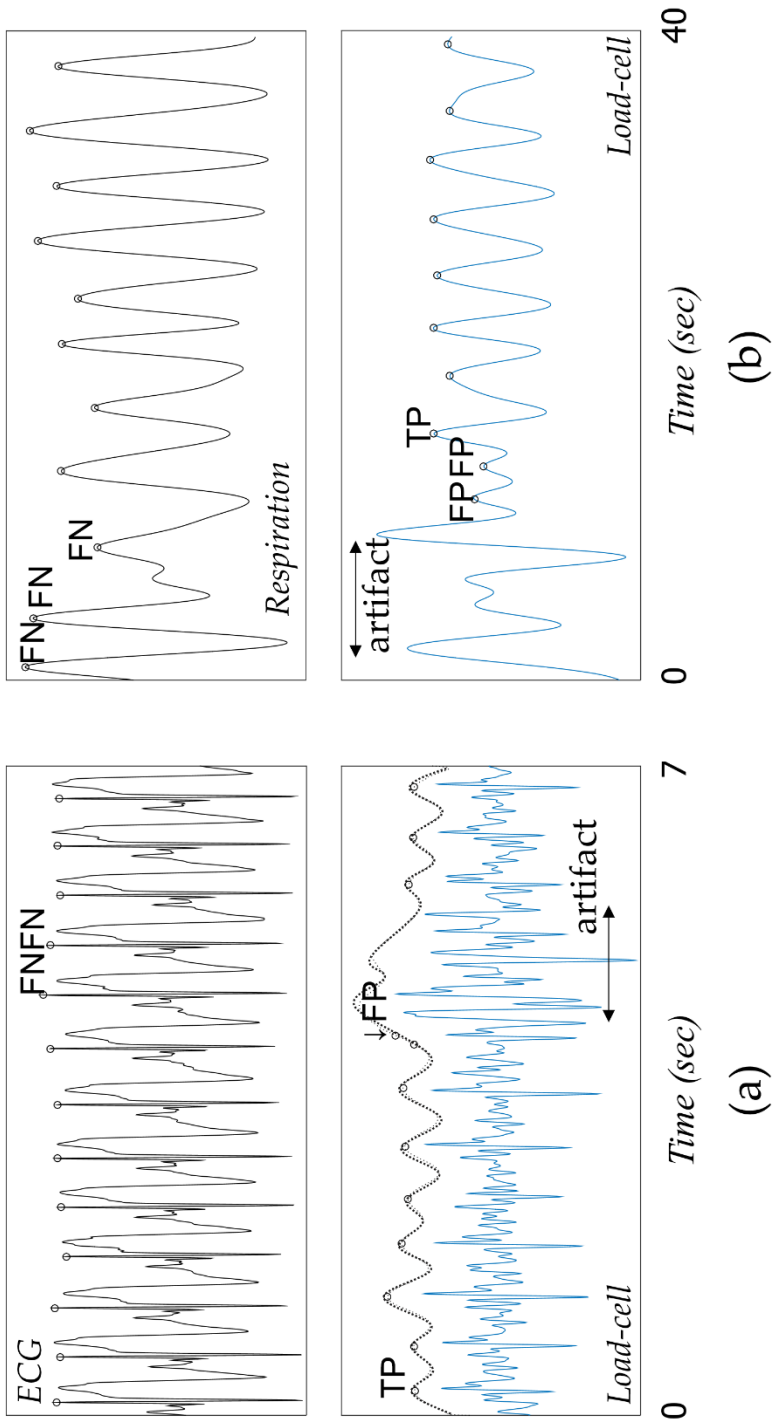


**Figure 20.** Manually annotated peak locations and automatic peak detection results of the load-cell sensor signal obtained by the developed algorithm in (a) HR analysis and (b) BR analysis (definitions of TP, FP, and FN are illustrated).

Figure 20 shows a comparison between the manually annotated peak locations and the automatic peak detection results of the load-cell sensor signal given by the developed algorithm. The detection rate (Dr) and positive predictive value (PPV) were calculated as follows:

$$\boldsymbol{Dr} = \frac{\boldsymbol{TP}_{(\boldsymbol{from\ load-cell\ signal})}}{\boldsymbol{Total\ number\ of\ beat}_{(\boldsymbol{ECG\ or\ Chest\ belt})}} \times \mathbf{100}\ (\%), \tag{6}$$

$$\mathbf{PPV} = \frac{\boldsymbol{TP}}{\boldsymbol{TP+FP}} \times \mathbf{100}\ (\%). \tag{7}$$

Second, the adequacy of the proposed algorithm with respect to regular HR or BR monitoring was evaluated. Our proposed algorithm uses a short analysis window of 5 s and 30 s lengths for HR and BR, respectively. For each non-overlapping 5 s (30 s) window, the difference and error between the mean HR (BR) derived from the load-cell sensor signal during that window and that derived from the ECG (respiratory signal from chest belt sensor) was computed. These differences and errors were then aggregated during each experiment. Finally, for each experiment, the mean absolute difference and mean absolute error were reported.

The coverage denotes the percentage of the signal that is automatically classified as clean. As mentioned above, to obtain reliable HR and BR signals from load-cell sensors, periods with poor signal quality are discarded during the signal quality check and optimum sensor selection step. The coverage was calculated as follows:

$$\begin{aligned}\mathbf{coverage}\ (\%) &= \frac{\boldsymbol{periods\ with\ clean\ signal}\ (\boldsymbol{s})}{\boldsymbol{Total\ periods\ of\ the\ experiment}\ (\boldsymbol{s})} \\ &= \frac{\boldsymbol{Total\ periods\ of\ experiment}\ (\boldsymbol{s}) - \boldsymbol{periods\ with\ artifact\ signal}\ (\boldsymbol{s})}{\boldsymbol{Total\ periods\ of\ the\ experiment}\ (\boldsymbol{s})}\end{aligned} \tag{8}$$

### 3.1.2.2. Results

We analyzed 13 records from four infant participants. The signals collected from the load-cell sensors include the components caused by cardiac activity and respiratory movement. To analyze the biological information, we also developed a MATLAB-based automatic algorithm that has been validated experimentally.

Table 3 and Table 4 show the results of the developed algorithm with respect to the beat locations for each experiment (see Chapter 3.1.2.1). The algorithm achieved an average detection rate of 76.16% (Table 3, HR) and 89.35% (Table 4, BR) and an average positive predictive value of 99.07% (Table 3, HR) and 96.22% (Table 4, BR).

**Table 3.** Performance evaluation results with respect to the beat locations in HR analysis.

| Record | Time (min) | Total Beat (ECG) | Total Beat (Load-Cell) | TP | FP | FN | FN * (Inevitable) | Detection Rate | PPV |
|---|---|---|---|---|---|---|---|---|---|
| A-1 | 12 | 995 | 677 | 666 | 11 | 329 | 141 | 66.93 | 98.38 |
| A-2 | 20 | 1785 | 1754 | 1748 | 6 | 37 | 3 | 97.93 | 99.66 |
| A-3 | 25 | 2298 | 1754 | 1730 | 24 | 568 | 288 | 75.28 | 98.63 |
| A-4 | 30 | 2868 | 1368 | 1327 | 41 | 1541 | 1027 | 46.27 | 97.00 |
| A-5 | 30 | 2270 | 2122 | 2120 | 2 | 150 | 107 | 93.39 | 99.91 |
| B-1 | 10 | 1114 | 444 | 435 | 9 | 679 | 307 | 39.05 | 97.97 |
| B-2 | 20 | 1968 | 1034 | 1009 | 25 | 959 | 453 | 51.27 | 97.58 |
| B-3 | 90 | 8651 | 7624 | 7566 | 58 | 1085 | 546 | 87.46 | 99.24 |
| C-1 | 11.9 | 1153 | 1063 | 1053 | 10 | 100 | 18 | 91.33 | 99.06 |
| C-2 | 178.8 | 18,481 | 15,399 | 15,244 | 155 | 3237 | 1402 | 82.48 | 98.99 |
| C-3 | 30 | 3235 | 2884 | 2867 | 17 | 368 | 114 | 88.62 | 99.41 |
| C-4 | 72 | 7874 | 5549 | 5516 | 33 | 2358 | 1101 | 70.05 | 99.41 |
| D-1 | 33 | 3598 | 1603 | 1592 | 11 | 2006 | 1962 | 44.25 | 99.31 |
| **Total** | **562.7** | **56,290** | **43,275** | **42,873** | **402** | **13,417** | **7469** | **76.16** | **99.07** |

*: FN (inevitable) represents the number of FN results that inevitably occur in an area determined to be an artifact.

**Table 4.** Performance evaluation results with respect to the beat locations in BR analysis.

| Record | Time (min) | Total Beat (Chest Belt) | Total Beat (Load-Cell) | TP | FP | FN | FN * (Inevitable) | Detection Rate | PPV |
|---|---|---|---|---|---|---|---|---|---|
| A-1 | 12 | Respiration was not recorded in these experiments | | | | | | | |
| A-2 | 20 | 396 | 379 | 377 | 2 | 19 | 0 | 95.20 | 99.47 |
| A-3 | 25 | 509 | 452 | 445 | 7 | 64 | 0 | 87.43 | 98.45 |
| A-4 | 30 | 344 | 262 | 230 | 32 | 114 | 0 | 66.86 | 87.79 |
| A-5 | 30 | 504 | 490 | 472 | 18 | 32 | 0 | 93.65 | 96.33 |
| B-1 | 10 | Respiration was not recorded in these experiments | | | | | | | |
| B-2 | 20 | 284 | 275 | 248 | 27 | 36 | 0 | 87.32 | 90.18 |
| B-3 | 90 | 1598 | 1575 | 1480 | 95 | 118 | 0 | 92.62 | 93.97 |
| C-1 | 11.9 | 301 | 273 | 271 | 2 | 30 | 0 | 90.03 | 99.27 |
| C-2 | 178.8 | 2699 | 2521 | 2409 | 112 | 290 | 0 | 89.26 | 95.56 |
| C-3 | 30 | 865 | 789 | 779 | 10 | 86 | 0 | 90.06 | 98.73 |
| C-4 | 72 | 1779 | 1580 | 1551 | 29 | 228 | 0 | 87.18 | 98.16 |
| D-1 | 33 | 824 | 786 | 765 | 21 | 59 | 0 | 92.84 | 97.33 |
| **Total** | **540.7** | **10,103** | **9382** | **9027** | **355** | **1076** | **0** | **89.35** | **96.22** |

*: FN (inevitable) results did not occur in BR analysis. Because the chest belt also consists of a force transducer, the reference signal is simultaneously interfered by a motion artifact. (We could not label the respiratory peak in both reference signals and load-cell signals.)

As in the case of many unobtrusive monitoring, the signals acquired by our load-cell system are prone to high-grade noise. The main artifacts are related to movement, which is an inevitable consequence of physiological monitoring. Thus, the most important aspect of signal analysis using unobtrusive sensors is to classify the good-quality signals. In our results, FN is defined as the failure to detect an existing ECG or respiratory peak. It is assumed that most FNs were the result of our algorithm automatically determining an analysis window to be a noise signal and discarding all peaks included in the window. We additionally investigate how FN results inevitably occur in the artifact area and are denoted as FN (inevitable).

However, the number of FPs and FNs gives a limited indication of the accuracy of the estimated HR and BR. We estimate that FN and FP

directly affect the lengths of their neighboring beat-to-beat intervals. Therefore, the overall quality of the estimated HR and BR monitoring was assessed by the mean difference and error in computing the intervals extracted from the load-cell sensors and the corresponding intervals given by the reference equipment.

Table 5 and Table 6 show the adequacy of the proposed algorithm with respect to regular HR or BR monitoring. On average, 73.79% and 84.25% of each signal was identified as being artifact-free and usable for HR or BR estimation, respectively. The results indicate that the mean errors of the estimated HR averaged over 5 s and the estimated BR averaged over 30 s were 2.55% and 2.66%, respectively.

**Table 5.** Comparison of HRs calculated from commercial device and proposed device.

| Records | Time (min) | Window (Number) ** | Coverage (%) | Mean HR from ECG (bpm) | Mean HR from Load-Cell (bpm) | Mean Difference * (bpm) | Mean Absolute Error * (%) |
|---|---|---|---|---|---|---|---|
| A-1 | 12 | 102 | 67.02 | 83.33 | 83.92 | 2.25 | 2.66 |
| A-2 | 20 | 250 | 98.39 | 89.29 | 89.46 | 1.07 | 1.18 |
| A-3 | 25 | 250 | 78.99 | 90.70 | 89.45 | 2.35 | 3.14 |
| A-4 | 30 | 202 | 52.61 | 89.65 | 86.64 | 3.96 | 5.24 |
| A-5 | 30 | 328 | 89.19 | 83.45 | 83.36 | 0.68 | 0.83 |
| B-1 | 10 | 52 | 41.91 | 110.31 | 106.15 | 5.19 | 5.82 |
| B-2 | 20 | 137 | 54.29 | 96.44 | 95.44 | 2.67 | 3.05 |
| B-3 | 90 | 1026 | 89.71 | 95.17 | 94.66 | 1.47 | 1.69 |
| C-1 | 11.9 | 137 | 92.18 | 96.84 | 97.14 | 1.38 | 1.43 |
| C-2 | 178.8 | 1928 | 85.82 | 101.66 | 100.53 | 2.24 | 2.58 |
| C-3 | 30 | 339 | 90.02 | 106.90 | 106.90 | 0.90 | 0.87 |
| C-4 | 72 | 655 | 72.54 | 107.17 | 106.53 | 1.95 | 1.94 |
| D-1 | 33 | 193 | 46.61 | 106.47 | 105.13 | 2.52 | 2.66 |
| **Average** | **43.28** | **430.69** | **73.79** | **96.72** | **95.79** | **2.20** | **2.55** |

*: Between HRs from ECG and BCG from load-cell data; **: Total number of short analysis windows that were used for HR analysis.

**Table 6.** Comparison of BRs calculated from commercial device and proposed device.

| Records | Time (min) | Window (Number) ** | Coverage (%) | Mean BR from Chest Belt (bpm) | Mean BR from Load-Cell (bpm) | Mean Difference * (bpm) | Mean Absolute Error * (%) |
|---|---|---|---|---|---|---|---|
| A-1 | 12 | Respiration was not recorded in these experiments | | | | | |
| A-2 | 20 | 40 | 97.53 | 19.81 | 19.80 | 0.19 | 0.96 |
| A-3 | 25 | 46 | 88.75 | 20.32 | 20.31 | 0.32 | 1.58 |
| A-4 | 30 | 29 | 46.77 | 17.57 | 18.41 | 0.95 | 4.75 |
| A-5 | 30 | 54 | 85.87 | 18.57 | 18.80 | 0.33 | 1.74 |
| B-1 | 10 | Respiration was not recorded in these experiments | | | | | |
| B-2 *** | 20 | 27 | 78.31 | 19.48 | 20.88 | 1.65 | 7.82 |
| B-3 | 90 | 163 | 87.95 | 19.17 | 19.75 | 0.63 | 3.08 |
| C-1 | 11.9 | 22 | 92.94 | 25.23 | 25.22 | 0.06 | 0.24 |
| C-2 *** | 178.8 | 200 | 82.36 | 25.80 | 25.68 | 0.60 | 2.42 |
| C-3 | 30 | 56 | 91.04 | 29.28 | 28.91 | 0.71 | 3.07 |
| C-4 | 72 | 128 | 85.76 | 25.22 | 25.28 | 0.31 | 1.21 |
| D-1 | 33 | 61 | 89.49 | 26.17 | 26.27 | 0.62 | 2.37 |
| **Average** | **49.15** | **75.09** | **84.25** | **22.42** | **22.66** | **0.58** | **2.66** |

*: Between BRs from chest belt and respiratory signal from load-cell data; **: Total number of short analysis windows that were used for BR analysis; ***: There was slight signal loss in the reference breathing signal. These sections were excluded in the analysis.

Some other related results cited in the literature are summarized in Table 7. However, it is impossible to make an objective comparison between our results and those in Table 7, which were obtained under different experimental circumstances. In particular, most of the results (Records 02–07) were obtained from adult subjects. The differences in subject details, recording times, and sensors used in the study are represented in this table.

**Table 7**. Performance summary of other related works.

| Record | Subjects and Detail | Sensor | Average Recording Time (min) | HR or BR | Mean Coverage (%) | Mean Difference (bpm) | Mean Absolute Error (%) | Reference |
|---|---|---|---|---|---|---|---|---|
| 01 | 1822±20 g of 5 premature infants (M = 1, F = 4) | PVDF | 10 | HR<br>BR | -<br>- | -<br>- | 4.41<br>8.24 | (62) |
| 02 | 26.5±0.7 year of 2 adults (M = 1, F = 1) | PVDF EMFi | 10 | HR | - | 1.75 ± 1.09 | - | (29) |
| 03 | 29±5 year of 16 adults (M = 9, F = 7) | Strain guages | 26.6 | HR | 95.94 ± 1.28 | - | 1.79 ± 0.86 | (5) |
| 04 | 23-40 year of 13 adults (M = 13) | Air-cell | 5 | HR<br>BR | -<br>- | 0.68 ± 0.77<br>0.50 ± 0.63 | 0.98 ± 0.49<br>2.85 ± 1.15 | (48) |
| 05 | 49-68 year of 28 adults (M = 15, F = 13) | PVDF | 540 | HR | 92.7 | - | 1.06 | (39) |
| 06 | 32.8±13.4 year of 8 healthy adults (M = 1, F = 7) | EMFi | 420 | HR | 84.53 ± 5.14 | - | 0.61 ± 0.21 | (6) |
| | 47.0±13.1 year of 25 insomnia patients (M = 13, F = 12) | | 393 | HR | 68.90 ± 15.33 | - | 0.83 ± 0.37 | |
| 07 | 25.69±7.13 year of 13 adults (M = 13) | PVDF | 10 | HR<br>BR | -<br>- | 0.61 ± 0.36<br>0.48 ± 0.35 | 0.99 ± 0.56<br>3.65 ± 2.89 | (42) |
| This study | | Load-cell | 43.3<br>49.2 | HR<br>BR | 73.79 ± 19.37<br>84.25 ± 13.45 | 2.20 ± 1.26<br>0.58 ± 0.44 | 2.55 ± 1.54<br>2.66 ± 2.11 | |

## 3.2. Algorithm for automatically analyzing unobtrusively measured ECG signal

We devised a small and lightweight ECG monitoring device, as described in Chapter 2.2. We developed software, including an algorithm that detects important ECG peaks, which is essential for HRV analysis. We verified the performance and reliability of the software. For verification, we obtained ECG signals for 41 subjects over an extended period to evaluate the efficacy of the algorithm in the detection of peaks.

### 3.2.1. Process flow of the algorithm

A QRS complex in an ECG signal indicates the depolarization state of a ventricle. The first positive signal is defined as the R-peak and the following negative signal is defined as the S-wave. We designed an algorithm to detect the QRS complex by detecting the R peaks and S waves, using the information on their amplitude and the temporal interval between waves; a diagram of this process is shown in Figure 21.

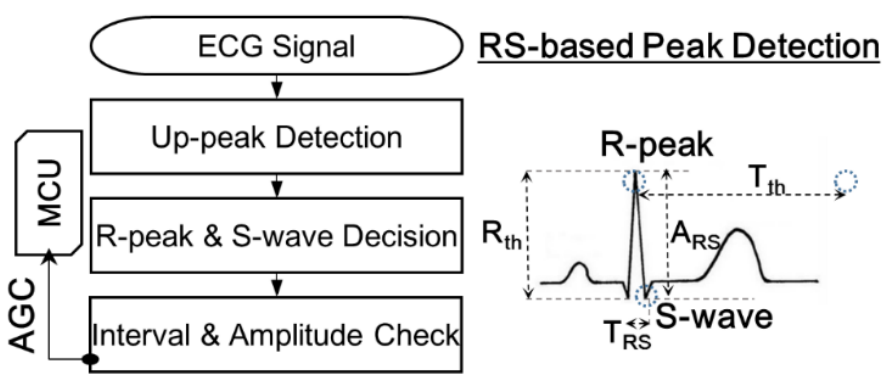


**Figure 21.** Flowchart of RS-based peak detection algorithm.

**(1) Up-peak detection:** In an ECG signal, up-peaks are detected by determining the point at which the slope changes from positive to negative, as well as the point of a local maximum. In our peak-detection algorithm, the R-peak and S-wave are determined from the following criteria.

**(2) R-peak amplitude ($R_{th}$):** The ECG measurement device we developed in this study includes an automatic gain control (AGC) function. The AGC function periodically analyzes the morphologic shape of the ECG signals and automatically adjusts the rate of amplification so that the amplitude of the R-peak exceeds a constant value. Letting $V_{lim}$ ($V_{lim}$ = -2048 to 2048) be the maximum range of the analog to digital conversion (ADC) value that can be expressed using the hardware, the amplitude of the R-peak must always satisfy equation 9.

$$R_{th} > \frac{V_{lim}}{2} \times 0.51 = A_{th} \tag{9}$$

**(3) Temporal interval between R-peaks considering refractory period:** Considering the refractory period of the heart, at least 200 ms is required for the successive generation of R-peaks. Therefore, the algorithm calculates the temporal interval between up-peaks with an amplitude in excess of $A_{th}$, detected as explained in (2). If the interval is less than 49 samples (= 191 ms), the peak is considered to be an abnormal peak due to noise, and is discarded.

**(4) Down-wave detection:** Beyond the peak that satisfies the criteria of (2) and (3), a window of 49 samples is applied. Among the data within the window, a down wave is determined by determining that point at which the

slope transitions from negative to positive and has a local minimum value.

**(5) Final decision:** The temporal interval ($T_{RS}$) and the amplitude ($A_{RS}$) between the up-peak and the down-wave determined using the methods described in (2) to (4) are measured. Using the developed device, we collected and analyzed ECG signals from over 30 subjects. As a result, we could set up an empirical threshold that normal ECG signals satisfy. Equation 10, below, shows the empirical threshold of $T_{RS}$ and $A_{RS}$.

$$T_{RS} \leq 78.125\ ms, A_{RS} \geq \frac{V_{lim}}{2} \times 0.87 \quad (10)$$

Through an analysis of the up-peak and down-wave information selected using this equation, R-peak was ultimately determined.

**• Automatic gain control (AGC)**

Some criteria included in the RS-based peak detection algorithm described in previous section are derived from the maximum range of the ADC value of the hardware ($V_{lim}$). We designed the algorithm to periodically analyze the morphologic form of the ECG to maintain a constant amplitude of the QRS complex so that the algorithm can function continuously. Through the application of the AGC, the amplification rate of ECG signals was periodically adjusted so that the R-peak is positioned at approximately 1000 ($V_{lim}$ = -2048 to 2048).

### 3.2.2. Performance evaluation

#### 3.2.2.1. Subjects and experimental method

To evaluate the efficacy of the algorithm at detecting peaks, 829 h of ECG data obtained from 41 subjects (about 20 h per subject) were obtained. The subjects went about their day-to-day activities after attaching the ECG monitoring device developed in this study to their torso.

Researchers with at least four years of experience labeled the peak information of the ECG signals. Two or more researchers analyzed the data as a team to maintain caution and objectivity in the labeling of the peak annotation. We used an internally developed MATLAB-based software tool that features manual R-peak marking or correction functions for ECG analysis.

Using the indicators of sensitivity (Se), the positive predictive value (PPV), and error (Er), the efficiency of the algorithm was statistically evaluated. These indicators were calculated by the methods defined by equations 11 to 13 (67).

$$\mathrm{Se} = \frac{TP}{TP + FN} \times 100\ (\%) \tag{11}$$

$$\mathrm{PPV} = \frac{TP}{TP + FP} \times 100\ (\%) \tag{12}$$

$$\mathrm{Er} = \frac{FP + FN}{TP + FN} \times 100\ (\%) \tag{13}$$

TP, FP, and FN indicate the following situations (TP: detected peak is a valid R-peak, FP: detected peak is not a valid R-peak, FN: failure to detect an existing R-peak). Se, PPV, and Er are statistical indexes used to evaluate

the following performances (Se: detection of R-peaks from a valid ECG, PPV: differentiation of peaks that are R-peaks and those that are not R-peaks from a valid ECG, Er: accuracy of the algorithm) (39).

#### 3.2.2.2. Results

We evaluated the performance of the peak-detecting algorithm using the ECG data obtained with the patch ECG monitoring system developed as part of this study (data are provided in Table 8). The algorithm shows the statistical results for Se = 99.29%, PPV = 100.00%, and Er = 0.71%, in comparison with the annotated work done manually by investigators on 829 h of ECG data. Additionally, the results of the other related algorithms cited in literature are summarized in Table 9 and compared to our results.

**Table 8.** Performance evaluation of proposed RS-based peak-detection method.

| Record | Duration | Number of beats | | | Se (%) | PPV (%) | Er (%) |
|---|---|---|---|---|---|---|---|
| | (hh:mm) | TP | FP | FN | | | |
| 01 | 21:15 | 104,434 | 0 | 1430 | 98.65 | 100.00 | 1.35 |
| 02 | 21:18 | 90,943 | 29 | 559 | 99.39 | 99.97 | 0.64 |
| 03 | 20:18 | 91,140 | 1 | 980 | 98.94 | 100.00 | 1.06 |
| 04 | 21:18 | 91,681 | 7 | 1727 | 98.15 | 99.99 | 1.86 |
| 05 | 21:11 | 103,308 | 6 | 913 | 99.12 | 99.99 | 0.88 |
| 06 | 21:15 | 96,683 | 0 | 33 | 99.97 | 100.00 | 0.03 |
| 07 | 21:16 | 100,495 | 2 | 587 | 99.42 | 100.00 | 0.58 |
| 08 | 11:09 | 35,462 | 3 | 2048 | 94.54 | 99.99 | 5.47 |
| 09 | 21:04 | 83,070 | 5 | 544 | 99.35 | 99.99 | 0.66 |
| 10 | 21:20 | 78,796 | 0 | 77 | 99.90 | 100.00 | 0.10 |
| 11 | 21:15 | 90,257 | 1 | 150 | 99.83 | 100.00 | 0.17 |
| 12 | 21:16 | 89,732 | 0 | 26 | 99.97 | 100.00 | 0.03 |
| 13 | 21:17 | 98,157 | 0 | 82 | 99.92 | 100.00 | 0.08 |
| 14 | 21:17 | 107,640 | 2 | 447 | 99.59 | 100.00 | 0.42 |
| 15 | 19:00 | 81,298 | 1 | 90 | 99.89 | 100.00 | 0.11 |
| 16 | 20:53 | 92,921 | 0 | 184 | 99.80 | 100.00 | 0.20 |
| 17 | 21:19 | 90,909 | 0 | 149 | 99.84 | 100.00 | 0.16 |
| 18 | 21:19 | 81,901 | 2 | 17 | 99.98 | 100.00 | 0.02 |
| 19 | 20:49 | 91,445 | 0 | 47 | 99.95 | 100.00 | 0.05 |
| 20 | 21:14 | 102,752 | 0 | 230 | 99.78 | 100.00 | 0.22 |
| 21 | 21:19 | 89,649 | 3 | 943 | 98.96 | 100.00 | 1.04 |
| 22 | 21:17 | 96,444 | 0 | 18 | 99.98 | 100.00 | 0.02 |
| 23 | 21:19 | 93,870 | 0 | 115 | 99.88 | 100.00 | 0.12 |
| 24 | 21:18 | 86,049 | 3 | 16 | 99.98 | 100.00 | 0.02 |
| 25 | 21:19 | 75,546 | 3 | 3485 | 95.59 | 100.00 | 4.41 |
| 26 | 20:54 | 89,701 | 0 | 61 | 99.93 | 100.00 | 0.07 |
| 27 | 21:14 | 90,903 | 1 | 100 | 99.89 | 100.00 | 0.11 |
| 28 | 21:17 | 82,640 | 16 | 4503 | 94.83 | 99.98 | 5.19 |
| 29 | 21:18 | 102,140 | 0 | 71 | 99.93 | 100.00 | 0.07 |
| 30 | 21:16 | 93,663 | 2 | 145 | 99.85 | 100.00 | 0.16 |
| 31 | 21:18 | 89,173 | 0 | 19 | 99.98 | 100.00 | 0.02 |
| 32 | 17:18 | 45,682 | 0 | 3 | 99.99 | 100.00 | 0.01 |
| 33 | 21:17 | 94,379 | 2 | 135 | 99.86 | 100.00 | 0.14 |
| 34 | 21:16 | 98,500 | 2 | 342 | 99.65 | 100.00 | 0.35 |
| 35 | 21:19 | 87,497 | 0 | 9 | 99.99 | 100.00 | 0.01 |
| 36 | 21:18 | 102,595 | 1 | 284 | 99.72 | 100.00 | 0.28 |
| 37 | 16:55 | 65,885 | 0 | 17 | 99.97 | 100.00 | 0.03 |
| 38 | 21:15 | 99,498 | 2 | 1262 | 98.75 | 100.00 | 1.25 |
| 39 | 21:16 | 92,162 | 0 | 199 | 99.78 | 100.00 | 0.22 |
| 40 | 20:45 | 69,753 | 7 | 630 | 99.10 | 99.99 | 0.91 |
| 41 | 21:18 | 85,688 | 21 | 3239 | 96.36 | 99.98 | 3.67 |
| **Total (TP, FP, FN) or Average (Se, PPV, Er)** | | **3,634,451** | **122** | **25,916** | **99.29** | **100.00** | **0.71** |

**Table 9.** Performance summary of other related works.

| Total beats | *TP* | *FP* | *FN* | *Se (%)* | *PPV (%)* | *Er (%)* | Reference |
|---|---|---|---|---|---|---|---|
| **(a) Performance comparison of algorithms tested by open source database (MITDB)** | | | | | | | |
| 109,494 | 109,401 | 91 | 93 | 99.92 | 99.92 | 0.17 | (65) |
| 109,494 | 109,398 | 103 | 96 | 99.91 | 99.91 | 0.18 | (51) |
| 108,494 | 108,323 | 97 | 171 | 99.84 | 99.91 | 0.25 | (67) |
| 109,494 | 109,241 | 393 | 253 | 99.77 | 99.64 | 0.59 | (2) |
| 116,137 | 115,860 | 507 | 277 | 99.76 | 99.56 | 0.68 | (45) |
| **(b) Performance comparison of algorithms tested by their own developed device** | | | | | | | |
| 27,012 | 27,001 | 40 | 11 | 99.96 | 99.85 | 0.19 | (55) |
| 7426 | 7253 | 138 | 173 | 97.67 | 98.13 | 4.19 | (35) |
| 67,143 | 65,116 | 1455 | 2027 | 96.98 | 97.81 | 5.19 | (2) |
| 7576 | 7103 | 37 | 473 | 93.76 | 99.48 | 6.73 | (2) |
| **(c) Performance results of algorithm for our developed device** | | | | | | | |
| 3,660,367 | 3,634,451 | 122 | 25,916 | 99.29 | 100.00 | 0.71 | - |

## 3.3. HRV analysis for processing unobtrusively measured signals

The HRV analysis methods can be divided into time and frequency domains. All of the HRV parameters presented in this paper were obtained by following the guidelines laid down by the Task Force of the ESC and NASPE. The intervals between the R-peaks (RRI) were derived from the detected R-peaks and ectopic beats that differ more than 20% from previous RRI were discarded. The HRV parameters for the period were calculated directly from these original RR interval time series. They include the mean HR (mean of the heart rate, in bpm), SDNN (standard deviation of all NN intervals, in ms), and RMSSD (the square root of the mean of the sum of the squares of the differences between adjacent NN intervals, in ms) (56).

Subsequently, after resampling at 4 Hz via piecewise cubic Hermite interpolating polynomial (PCHIP) interpolation, the HRV parameter for the

frequency was calculated. Irregularly time-sampled signals should be produced as an even sample time series prior to spectrum estimation to prevent the generation of additional harmonic components in the spectrum (44). While a standard rule of the RR interval resampling frequency is not defined, 4 Hz has generally been adopted in most HRV reports (49,50). The resampling rate needs to be chosen according to the Nyquist criterion; thus, 4 Hz is acceptable for the case when the RR tachogram remains below 120 bpm (*i.e.*, 2 Hz) (12). According to Singh *et al.*, "This is an appropriate resampling rate for the study of autonomic regulation, since it enables the computation of reliable spectral estimates between DC and 1 Hz, which represents the frequency band within which the ANS has a significant response (50)." The PSD results from the FFT were divided by the frequency range. The low frequency (LF) and high frequency (HF) components were indicated as frequency ranges of 0.04 to 0.15 Hz, and 0.15 to 0.4 Hz, respectively. The sum of each component was normalized and indicated as norm LF and norm HF. The ratio of the normalized component was expressed as LF/HF (53). The HF component mainly reflects the activity of the vagus nerve. Some investigators claim that the LF component indicates the quantitative activity of the sympathetic nerve while others argue that it reflects the activity of both the sympathetic and parasympathetic nerves. Regardless, the LF/HF ratio is commonly used as an index for the vagal balance, reflected according to the activity of sympathetic nerve (8,53).

### 3.3.1. Optimum HRV algorithm selection in data missing simulation

There are many HRV analysis methods. In many cases, these methods were validated in a resting state without missing data. However, with signals that

were obtained using unobtrusive sensors like ours, regular use during everyday life can lead to missing data related to various types of noise such as motion artifacts. Because different methods have various errors with missing data, we planned a simulation study to determine the most appropriate HRV analysis method assuming a condition in which some data was missing.

We used 169 samples of actual ECGs without missing data. To simulate the missing data, we removed some parts of the intervals both randomly and consecutively. In fact, this type of situation, with missing data, can occur during long-term daily-life physiological signal monitoring. After 500 repetitions, we analyzed the results with various spectral analysis methods: the Periodogram method, the Welch method, the Burg method, with linear, spline, and PCHIP interpolation, and the Lomb-Scargle method. Missing data causes differences between the parameters relative to the original condition. To assess this error, we normalized the errors. Using confidence intervals, this method allows a proper HRV analysis comparison with a wide range of parameters. We sought to choose the most appropriate HRV analysis method in a condition in which data is missing.

Figure 22 shows the results of the missing-data simulation study. In normal situations without any artificial noise, we can use all of these methods. However, given the existence of missing data caused by various types of noise, we need to consider performance differences according to PSD and interpolation methods. After increasing the percentage of missing data from 1% to 20%, the minimum errors were calculated, as indicated in the yellow highlighted areas in Figure 22. The Burg autoregressive (AR) model-based method with PCHIP interpolation shows the minimum error in a condition characterized by missing data.

| (500 repeat) NE (%) | Periodogram | | | Welch | | | Pburg | | | Lomb |
|---|---|---|---|---|---|---|---|---|---|---|
| | Linear | Spline | Pchip | Linear | Spline | Pchip | Linear | Spline | Pchip | |
| 1% missing | 0.2165 | 0.1293 | 0.1799 | 0.2121 | 0.1565 | 0.1843 | 0.2141 | 0.1386 | 0.1770 | 1.3090 |
| 2% missing | 0.3584 | 0.3608 | 0.3404 | 0.3561 | 0.3942 | 0.3392 | 0.3513 | 0.3718 | 0.3191 | 1.8538 |
| 3% missing | 0.4795 | 0.8213 | 0.4941 | 0.4856 | 0.8030 | 0.4917 | 0.4592 | 0.7966 | 0.4560 | 2.2980 |
| 4% missing | 0.5707 | 1.5257 | 0.6108 | 0.5968 | 1.4398 | 0.6173 | 0.5448 | 1.4652 | 0.5515 | 2.7372 |
| 5% missing | 0.6619 | 2.5434 | 0.6909 | 0.6666 | 2.2213 | 0.6969 | 0.6295 | 2.5928 | 0.6217 | 3.2106 |
| 6% missing | 0.7761 | 3.5210 | 0.7755 | 0.7581 | 3.0542 | 0.7708 | 0.6970 | 3.8720 | 0.6675 | 3.6461 |
| 7% missing | 0.8804 | 4.4184 | 0.8499 | 0.8727 | 3.8731 | 0.8488 | 0.7762 | 5.2572 | 0.7111 | 4.0778 |
| 8% missing | 1.0112 | 5.5792 | 0.9606 | 1.0074 | 4.8850 | 0.9680 | 0.9029 | 7.1625 | 0.8056 | 4.5246 |
| 9% missing | 1.1068 | 6.6324 | 1.0341 | 1.1087 | 5.8227 | 1.0523 | 0.9858 | 8.7182 | 0.8669 | 4.9723 |
| 10% missing | 1.2036 | 7.5332 | 1.1059 | 1.2012 | 6.7085 | 1.1277 | 1.1034 | 10.0251 | 0.9526 | 5.3826 |
| 11% missing | 1.3119 | 8.0673 | 1.1885 | 1.3039 | 7.3177 | 1.2104 | 1.1895 | 11.1006 | 1.0225 | 5.7769 |
| 12% missing | 1.3783 | 8.3344 | 1.2256 | 1.3741 | 7.8315 | 1.2522 | 1.2823 | 11.1101 | 1.0754 | 6.1567 |
| 13% missing | 1.4751 | 8.6481 | 1.2584 | 1.4454 | 8.1934 | 1.2925 | 1.3636 | 12.1273 | 1.1155 | 6.5128 |
| 14% missing | 1.6276 | 8.4772 | 1.3875 | 1.5928 | 8.6145 | 1.4101 | 1.5057 | 12.1918 | 1.2276 | 6.8356 |
| 15% missing | 1.7400 | 8.4277 | 1.4667 | 1.7110 | 8.6989 | 1.4933 | 1.6206 | 12.0985 | 1.3074 | 7.1604 |
| 16% missing | 1.8993 | 7.9863 | 1.5963 | 1.8573 | 8.8577 | 1.6051 | 1.7658 | 12.0601 | 1.4187 | 7.4757 |
| 17% missing | 2.0133 | 7.5232 | 1.6454 | 1.9349 | 8.8230 | 1.6596 | 1.8471 | 12.1031 | 1.4722 | 7.7943 |
| 18% missing | 2.1647 | 7.1677 | 1.7698 | 2.0713 | 8.9536 | 1.7633 | 1.9794 | 12.4748 | 1.5586 | 8.0788 |
| 19% missing | 2.3025 | 6.8952 | 1.8933 | 2.2294 | 9.0678 | 1.8957 | 2.0990 | 13.3285 | 1.6593 | 8.3850 |
| 20% missing | 2.4810 | 6.5962 | 2.0218 | 2.3755 | 9.0684 | 2.0173 | 2.2449 | 13.9942 | 1.7607 | 8.6910 |

**Figure 22.** Results of the missing-data HRV simulation study.

### 3.3.2. Stress assessment using HRV parameters

To verify the performance and practicality of the new device, we compared the HRV analysis results. This experiment was undertaken with 17 subjects (average age 27.8 (± 3.1)), obtaining the ECG from both a commercial device and the newly developed device in a mentally stressful situation. The test consisted of a resting state (5 min) - Stroop test (5 min) - mental arithmetic task (5 min) sequence. The Stroop test assesses color–word interference. Test participants are asked to respond with the name of a color that is different from the meaning of a colored word. In the mental arithmetic task, subjects were asked to repeatedly subtract 13 from 1079. Subjects were not allowed to use their fingers or pens, and were only allowed to perform the calculations in their heads (Figure 23).

ECG signals from both a commercial device and the newly developed device were measured simultaneously (*i.e.*, concurrent data acquisition) for all mental stress states to prevent debate regarding confounding effects like learning. After obtaining the ECG from both devices, the HRV of the time and frequency domain was analyzed in a similar manner as described in the previous section (HRV analysis). The reliability of the new device was evaluated by comparing the results obtained with the two devices.


(a)

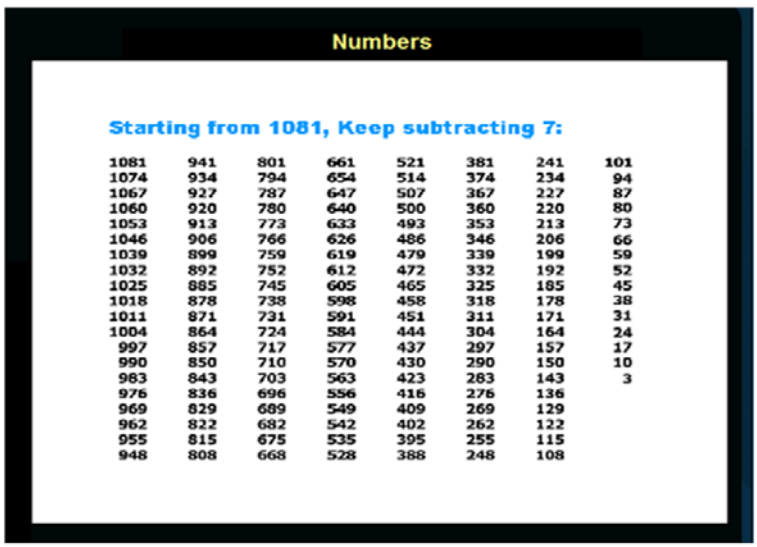


(b)

**Figure 23.** Stress inducing tasks (a) Stroop test (b) mental arithmetic task.

Figure 24 compares an HRV analysis of the ECG signals as obtained with conventional means and the newly developed device for the subjects undertaking an experiment inducing mental stress. When an individual is anxious or excited, the sympathetic nervous system is activated, increasing the LF value among the HRV indexes. Moreover, when an individual is angry, concerned, or afraid, the parasympathetic nervous system is deactivated, leading to a decrease in the HF value (8,57). Therefore, our identification of the increased LF/HF ratio in stressed subjects is consistent with the general physiological principles of ANS imbalance. We found that, for subjects placed in stressful situations such as taking the Stroop test or a mental arithmetic task, the LF/HF ratio, which reflects the balance state of the ANS, increased significantly. Table 10 shows the detailed HRV results. The variance of LF/HF ratio by different spectral analysis methods are compared in Table 11.

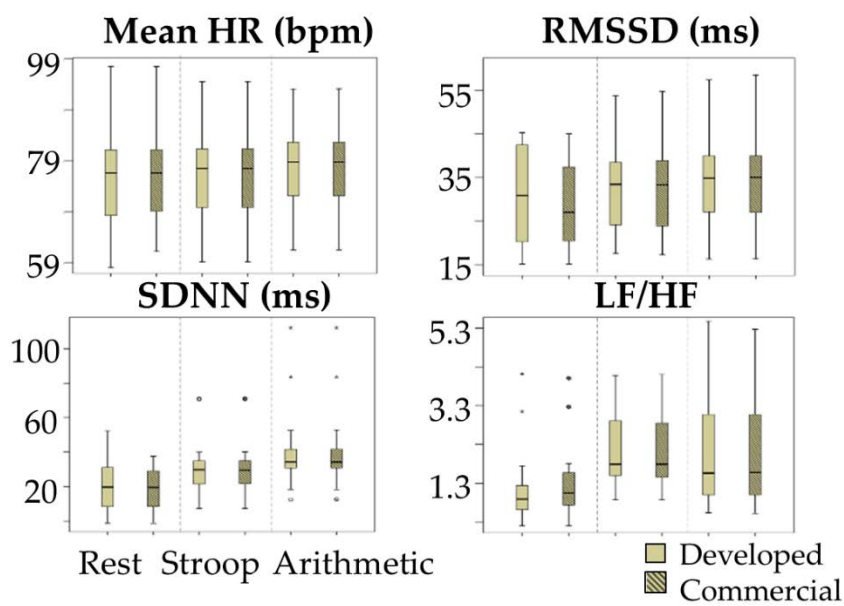


**Figure 24**. Comparison of HRV parameters under stressful conditions.

**Table 10.** Changes of HRV parameters under stressful conditions.

| HRV parameter | Rest | Stroop test | Arithmetic task |
|---|---|---|---|
| **mean HR** | 74.15 | 76.45 | 78.85 |
| **SDNN** | 40.99 | 56.31 | 54.81 |
| **RMSSD** | 35.01 | 33.41 | 31.01 |
| **LF/HF ratio** | 1.31 | 2.17 | 2.10 |
| **Triangular index** | 10.67 | 12.21 | 13.53 |
| **TINN** | 169.1 | 220.3 | 267.4 |

**Table 11.** Results of LF/HF ratio using various spectral analysis methods.

| LF/HF ratio | Rest | Stroop test | Arithmetic task |
|---|---|---|---|
| **Periodogram** | 1.31 ± 1.00 | 2.17 ± 0.86 | 2.10 ± 1.41 |
| **Welch** | 1.20 ± 1.02 | 2.17 ± 0.97 | 2.16 ± 1.44 |
| **Burg** | 1.30 ± 1.19 | 2.15 ± 0.98 | 2.15 ± 1.38 |

Also, when differences in the HRV analysis results obtained with the conventional and newly developed device were plotted as a box plot, equivalent results were obtained, confirming the measuring accuracy of the new device. Statistically, using linear regression to compare the results from both devices, the regression value was over 0.99 for every HRV parameter. This signifies that the measured results are identical in the two devices.

# Chapter 4

# Discussion

**• Physiological signal monitoring for infants based on load-cell sensors**

After the basic concept of BCG was introduced in 1877, unobtrusive physiological measurement using ballistocardiography technology has become a topic of interest that has attracted much research attention. Recently, a review of numerous studies on BCG has been presented in (26). However, it is rare to find studies that have focused on monitoring the biological signals of infants. As mentioned in the introduction section, ballistocardiography technology could play a more important role when applied to infants, who are difficult to physically confine. We believe that the proposed device and algorithm presented herein are essential for realizing the unobtrusive monitoring of infants.

The performance of the developed BCG system is described in Chapter 2.1 (hardware) and Chapter 3.1 (software). In this study, we developed a load-cell installed bed to measure the cardiac activity, respiration, and movement of infants, as illustrated in Figure 5. The basic concepts of the present system, including the load-cell's arrangement and the circuit design, are based on our former system (10,32). However, the detailed

hardware specifications differ to account for the relatively low weight of the infant subjects. At the beginning of our study, we attempted to revamp an existing monitoring system. This system was built with four load-cell sensors (MNC-100L, CAS, Yangju-si, Gyeonggi-do, Korea) installed under the legs of the bed. The capacity of the load-cell was 100 kg, and its rated output is 2 mV/V. Although it was well suited for detecting the subtle body vibrations of adults, we could not discern any useful signal for applying the same system to infants. We suppose that the high capacity of the load-cell for covering the entire weight, including that of the bed, leads to lower sensitivity, which is not appropriate for measuring the subtle body vibrations of infants. Considering the few characteristics that affect the load-cell sensitivity (see Chapter 2.1), it is relatively easy to reduce the capacity of the load-cell. We designed a simple load-cell (capacity of 6 kg) system while retaining the essential functions, thus we expect a theoretical system capacity of only 24 kg for realizing an improvement in the sensitivity. In the commercialization stage, we plan to incorporate our developed device into the body of a commercial infants' bed.

We could finally measure cardiac and respiratory signals by using load-cell sensor-based bed system. Figure 9 shows a partial example of the monitored signals measured from a 19-month-old male subject. According to the observational record, the subject lay down in bed in a somewhat diagonal direction. His head was located near sensor 1, the region of the right shoulder and heart was located near sensor 2, the region of the hip and right leg was located near sensor 3, and the left leg was located near the middle of sensors 3 and 4 (please refer to the sensor locations in Figure 5a). Because the chest and stomach are biased to the region of sensors 2 and 3, the respiratory signals are observed as relatively distinct shapes in the corresponding

channels. Furthermore, there are phase differences in the recorded respiratory signals between sensors 2 and 3. As already discussed in several literatures, the respiration signals could have phase differences caused by the different movement directions depending on the longitudinal arrangement of sensors (33). As mentioned above, sensors 2 and 3 are located near the chest and stomach, respectively. Thus, different timings of expansion and contraction of the stomach and thorax are reflected in the signal (43).

The amplitudes of the BCG signals vary depending on their location, and the BCG waveform recorded from sensor 2 shows maximum IJ amplitude (Figure 9h). Because sensor 2 is the nearest to the heart, it can be assumed that the distance between the vibration source and the sensor affects the signal attenuation. Clean BCG waveforms are observed in the signal from sensor 1, and these are particularly less interfered by respiratory movements. In the experiment, the subject's head was located near sensor 1; we assume that this posture feature is related to the phenomena. We assume that the location of the head affects the interference of the respiratory movement. The relative dominance of cardiac fluctuations in the area near the head is often found from our past experiences, even research approaches for embedding force transducers in pillows to monitor cardiac cycles have been reported (9).

The biggest challenge in monitoring the HR using BCG signal is finding features. Because it is generally known that the J peak has the largest amplitude, algorithms for estimating the heart rate by detecting the J peak have been developed. However, unlike an ECG signal having one special fiducial point, that is, QRS complex, the several waveform peaks of the BCG signal (labeled H through N) have similar size and shape. Furthermore,

because the BCG signal waveform varies a lot depending on the sensor used and the position at which it was measured, it is not easy to develop a robust algorithm that considers all these characteristics. Brüser *et al.* developed and verified a new algorithm that can measure the beat-to-beat interval that corresponds to a heartbeat, unlike the conventional method for finding the location of the J peak (6). It is difficult to expect the J peak to be dominant for an infant BCG signal processed in this study because of the nature of a premature heart. We also thought that it was more important to find the corresponding interval to obtain the correct average HR instead of finding the exact location of the J peak. Thus, we developed a modified algorithm based on Brüser's method.

In this study, the sensor selection process that detects valid signals from multiple sensors was considered important, unlike in previous studies. By combining the advantages of existing methods (4,42), we developed an automatic sensor selection method using an indicator that can estimate the artifact level using the auto correlation coefficient value and area rate of PSD. We assessed the coverage and mean relative error of experiments by varying the threshold value of the indicator that decides the artifact level. There is a trade-off: if the threshold value is set high, the error as well as the coverage decrease because of the increased number of dropped signals. The threshold value from our empirical experience based on the result of this study is 0.65 for HR analysis and 1.25 for BR analysis.

The performance of our algorithm was evaluated using experimental results, and it is summarized in Tables 3 – 6. Table 3 and Table 4 show the result of evaluating how precisely the algorithm can detect the peak location in terms of TP, FP, and FN. The peak was detected at 76.16% and 89.35% in contrast to the reference signal (ECG for heartbeat and chest-

belt for respiration, respectively). The increased number of FNs in HR analysis is inevitable because of the nature of the algorithm, which automatically runs the entire process of checking the quality and selecting the optimum sensor. In fact, the inevitable number of FNs that occurred in the area determined to be an artifact area was around 55% (=7469/13,417) of the total number of FNs in the HR analysis. This serves as contrasting evidence that only a clear signal was analyzed using a strict standard that is underpinned by high PPV values. Apart from traditional methods for finding the location of the J peak, the detected beat-to-beat intervals that correspond to the heartbeat and respiratory cycle were evaluated by averaging the error of the preset window. The averaged relative differences and errors are summarized in Table 5 and Table 6, respectively.

We also summarized several related studies in Table 7. The application of BCGs to infants is very rare, and it is difficult to directly compare our method with other BCG-based techniques applied to a similar group of subjects. Erkinjuntti *et al.* reported the feasibility of the static charge sensitive bed method for the monitoring of around 40 neonates (15). However, they showed just a partial example of the simultaneous recording of signals and did not present algorithms for HR and BR analysis. Wang *et al.* investigated a polyvinylidene difluoride (PVDF) piezoelectric film sensor system; however, their experiments only lasted 10 min on average, and their method showed only mean peak detection errors including FP and FN. Thus, we could estimate the accuracy of the estimated HR and BR signals to have mean peak detection errors of 8.24% and 4.41%, respectively (62). For adults, BCG-derived HR and BR measurements have achieved lower errors than in our study. Other sensors such as a static charge sensor, piezoelectric sensor (PVDF and EMFi), acceleration sensor, and optical sensor have been used for

detecting BCG signals when lying down in bed. A direct comparison is difficult because each method has its own advantages. However, because the load-cell sensor used in this study has the stability in terms of long-term monitoring with high accuracy as well as can simultaneously detect static/dynamic changes, we decided that it was suitable for monitoring the biological signals of infants for a long period of time when they were lying in bed. Studies for comparing the features of various sensors processed with standardized conditions in a controlled situation are needed.

**• Portable ECG monitoring patch for health management in daily life**

In this study, we suggested a new system for measuring ECG, using a patch with minimized electrode arrays as an alternative to a conventional portable ECG measuring system in order to improve portability, wear comfort, and accuracy of measurement when the subject is moving.

The performance of the developed ECG system is described in Chapter 2.2 (hardware) and Chapter 3.2 (software). In general, when evaluating the performance of an algorithm, open source data such as the MIT-BIH database are used to objectively evaluate its performance and reliability (40,45). However, in this study, the algorithm we developed was based on the AGC and the indigenous threshold of the maximum amplitude that can be expressed on the developed hardware. Thus, this algorithm is optimized to process only data obtained with the newly developed device.

The results of the ECG measurements and peak detection tests performed as the subjects performed their day-to-day lives showed an acceptable level of performance, given a sufficient number of subjects (Table 8). However, there are some limitations. The algorithm adopted for this study can analyze only the data acquired from our hardware. Although we

summarize the performance comparison in Table 9, it was impossible to make an objective comparison with other algorithms that differ in their experimental circumstances.

The method in which we obtained an ECG using a commercial device is similar to the common use of the conventional Holter device. We connected the leads and the device with wires and anchored the wires to the body of the subject with tape. However, even with the wires firmly fixed, the ECG signal quality was often disturbed as the wires moved depending on the subject's body movements as he or she walked or performed other actions. According to one study, the ratio of motion peaks to normal peaks was estimated as being about 10% when the ECG was taken from a freely moving patient using the Holter system. For this reason, the ECGs obtained using Holters were limited, and algorithms used to eliminate noise from the data have been actively developed (58). As important as it is to detect and exclude generated noise from the analysis, it is even more important to reduce the occurrence of noise itself.

We evaluated cardiac activities using the developed device and a conventional device under conditions that represent day-to-day activities and analyzed the SNRs of both ECGs to evaluate the amount of noise generation in the two devices (Figure 12). In circumstances involving little action, reasonable SNR estimation values were observed for both devices. When we increased the motion of the subjects, we found that the new device was relatively less affected by motion noise. It is obvious that the movement of the wire connecting the leads and the device add to the presence of noise in the conventional equipment. Generally, devices used to acquire ECG data during day-to-day activities are susceptible to diverse noise such as power noise, respiratory noise, and muscle noise.

From the results, we expect our device to be capable of obtaining more stable and simpler ECG measurements for day-to-day activities, including those with moderate amounts of movement, (*e.g.*, walking at 5 km/h). This improvement results from efforts to minimize noise artifacts from both the software preprocessing the signals and the hardware, which was achieved by incorporating the wires connecting the leads to the device into the integral patch. Therefore, we anticipate that the new device will be useful for ECG monitoring during real-life activities while still being able to measure stable and credible waves.

Moreover, we analyzed the activities of ANS while the subject was subjected to a stressful situation in order to examine the performance and practicality of the device designed in this study (see Chapter 3.3.2). The HRV parameters were significantly different between normal and stressful conditions. This was clearly distinguishable using the new device.

There is currently an increased demand for HRV analysis in a wide range of user environments. Therefore, technology using a patch electrode and a measuring module to measure ECG is very well suited to application as a health monitoring system. Specifically, the target market for the developed device will likely be those related to sleep, chronic disease, or any applications that have a need for long-term ECG monitoring. Also, tests related to the adoption of Bluetooth low energy (BLE) wireless communication are being undertaken to keep pace with the convergence of the Internet of Things (IoT) and mobile health (m-Health). The developed device has already been granted Korea Food & Drug Administration (KFDA) certification and will be granted CE and FDA 510(k) in the future.

# Chapter 5

# Conclusion

Since demand for health monitoring systems with unobtrusive sensors is increasing all over the world, devices specifically designed for evaluating the physiological status of the human body are needed. To this end, this dissertation is dedicated to summarizing our research of monitoring cardiorespiratory activities by means of unobtrusive sensing methods based on technologies of ECG and BCG measurement.

First, we designed a load-cell-based physiological signal monitoring bed for infants and investigated whether BCG and respiratory signals could be obtained accurately. By analyzing the data derived from 13 experiments with four infants, we verified that the proposed BCG-based technology could estimate both HR and BR information with average errors of 2.55% and 2.66%, respectively, compared with reference equipment. Although our results demonstrate that the proposed method shows acceptable performance, there are two main limitations in our study, insufficient recording time and too few measurements. Future research projects should increase the number of subjects in the experiment and extend the age distribution. The recording times should be increased to cover various

occurrences of all possible types and combinations of movements during sleep and wakefulness. However, despite these limitations, the preliminary results provide a positive feasibility for future studies of BCG-based measurements in infants. We believe that the development of the proposed device and algorithm presented here is an essential step toward substantiating the unobtrusive physiological measurement for infants. The proposed technology could be used for the continuous observation of infants, especially to detect respiratory distress and cardiac abnormalities. We also expect this technology to be used for extensive applications in the field of sleep research for analyzing sleep efficiency and sleep patterns of infants.

Second, we developed a smart patch device for electrocardiography. The smart patch measures ECG using three electrodes integrated into the patch, filters the measured signals to minimize noise, performs analog to digital conversion (ADC), and detects R-peaks. The measured raw ECG data and the interval between the detected R-peaks can be recorded to enable long-term HRV analysis. Experiments were performed to evaluate the performance of the built-in R-wave detection, robustness of the device under motion, and applicability to the evaluation of mental stress. The R-peak detection results obtained with the device exhibited a sensitivity of 99.29%, a positive predictive value of 100.00%, and an error of 0.71%. The device also exhibited less motional noise than conventional ECG recording, being stable up to a walking speed of 5 km/h. When applied to mental stress analysis, the device evaluated the variation in HRV parameters in the same way as a normal ECG does, with very little difference. This device can help users better understand their state of health and provide physicians with more reliable data for objective diagnosis.

# Reference


1. Abbas AK, Heimann K, Jergus K, Orlikowsky T, Leonhardt S. Neonatal non-contact respiratory monitoring based on real-time infrared thermography. *Biomed Eng Online* 2011; 10: 93.
2. Adnane M, Jiang Z, Choi S. Development of QRS detection algorithm designed for wearable cardiorespiratory system. *Comput Meth Prog Bio* 2009; 93: 20–31.
3. Barrera-Ramirez J, Bravi A, Green G, Seely AJ, Kenny GP. Comparison of heart and respiratory rate variability measures using an intermittent incremental submaximal exercise model. *Appl Physiol Nutr Metab* 2013; 38: 1128-36.
4. Böhm A, Brüser C, Leonhardt S. A novel BCG sensor-array for unobtrusive cardiac monitoring. *Acta Polytech* 2013; 53: 862–7.
5. Brüser C, Stadlthanner K, de Waele S, Leonhardt S. Adaptive beat-to-beat heart rate estimation in ballistocardiograms. *IEEE Trans Inf Technol Biomed* 2011; 15: 778–86.
6. Brüser C, Winter S, Leonhardt S. Robust inter-beat interval estimation in cardiac vibration signals. *Physio Meas* 2013; 34: 123–38.
7. Buckles D, Aguel F, Brockman R, Cheng J, Demian C, Ho C, Jensen D, Mallis E. Advances in ambulatory monitoring: regulatory considerations. *J Electrocardiol* 2004; 37: 65–7.
8. Castaldo R, Melillo P, Bracale U, Caserta M, Triassi M, Pecchia L. Acute mental stress assessment via short term HRV analysis in healthy adults: a systematic review with meta-analysis. *Biomed Signal Process Control* 2015; 18: 370–7.

9. Chen W, Zhu X, Nemoto T, Kanemitsu Y, Kitamura K, Yamakoshi K. Unconstrained detection of respiration rhythm and pulse rate with one under-pillow sensor during sleep. *Med Biol Eng Comput* 2005; 43: 306–12.
10. Choi BH, Chung GS, Lee JS, Jeong D-U, Park KS. Slow-wave sleep estimation on a load-cell-installed bed: A non-constrained method. *Physiol Meas* 2009; 30: 1163–70.
11. Choi S, Jiang Z. A novel wearable sensor device with conductive fabric and PVDF film for monitoring cardiorespiratory signals. *Sens Actuator A Phys* 2006; 128: 317–26.
12. Clifford GD, Tarassenko L. Quantifying errors in spectral estimates of HRV due to beat replacement and resampling. *IEEE Trans Biomed Eng* 2005; 52: 630–8.
13. DiBlasi RM. Neonatal noninvasive ventilation techniques: Do we really need to intubate? *Resp Care* 2011; 56: 1273–97.
14. Dziuda Ł, Skibniewski FW. A new approach to ballistocardiographic measurements using fibre Bragg grating-based sensors. *Biocybern Biomed Eng* 2014; 34: 101-16.
15. Erkinjuntti M., Vaahtoranta K, Alihanka J, Kero P. Use of the SCSB method for monitoring of respiration, body movements and ballistocardiogram in infants. *Early Hum Dev* 1984; 9: 119–26.
16. Flandrin P, Gonçalvè P, Rilling G. Detrending and denoising with empirical mode decompositions. Proceedings of 12th European Signal Processing Conference; 2004 Sep 6-10; Vienna, Austria. IEEE; c2004. p. 1581-4.

17. Fletcher RR, Dobson K, Goodwin MS, Eydgahi H, Wilder-Smith O, Fernholz D, Kuboyama Y, Hedman EB, Poh M-Z, Picard RW. iCalm: Wearable sensor network architecture for wirelessly communicating and logging autonomic activity. *IEEE Trans Inf Technol Biomed* 2010; 14: 215–23.
18. Gomez-Clapers J, Serra-Rocamora A, Casanella R, Pallas-Areny R. Toward the standardization of ballistocardiography systems for J-peak timing measurement. *Measurement* 2014; 58: 310-6.
19. González-Landaeta R, Casas O, Pallàs-Areny R. Heart rate detection from an electronic weighing scale. *Physiol Meas* 2008; 29: 979–88.
20. Hafner N, Mostafanezhad I, Lubecke VM, Boric-Lubecke O, Host-Madsen A. Non-contact cardiopulmonary sensing with a baby monitor. Proceedings of 29th Annual International IEEE EMBS Conference; 2007 Aug 23-26; Lyon, France. IEEE; c2007. p. 2300-2.
21. Heart smart [Internet]. Boston Scientific Corporation. Available from http://www.lifebeatonline.com/en-US/explore-heart-conditions/heart-smart.html
22. Hu Y, Kim EG, Cao G, Liu S, Xu Y. Physiological acoustic sensing based on accelerometers: a survey for mobile healthcare. *Ann Biomed Eng* 2014; 42: 2264–77.
23. Inan OT, Etemadi M, Paloma A, Giovangrandi L, Kovacs GTA. Non-invasive cardiac output trending during exercise recovery on a bathroom-scale-based ballistocardiograph. *Physiol Meas* 2009; 30: 261–74.
24. Inan OT, Etemadi M, Wiard RM, Giovangrandi L, Kovacs GTA. Robust ballistocardiogram acquisition for home monitoring. *Physiol Meas* 2009; 30: 169–85.

25. Inan OT, Etemadi M, Wiard RM, Kovacs GTA, Giovangrandi L. Novel methods for estimating the ballistocardiogram signal using a simultaneously acquired electrocardiogram. Proceedings of 31th Annual International IEEE EMBS Conference; 2009; Sep 3-6; Minneapolis, MN, USA. IEEE; c2009. p. 5334–47.
26. Inan OT, Migeotte P-F, Park K-S, Etemadi M, Tavakolian K, Casanella R, Zanetti J, Tank J, Funtova I, Prisk GK, Rienzo MD. Ballistocardiography and seismocardiography: a review of recent advances. *IEEE J Biomed Health Inform* 2015; 19: 2168-94.
27. Inan OT, Park D, Giovangrandi L, Kovacs GTA. Noninvasive measurement of physiological signals on a modified home bathroom scale. *IEEE Trans Biomed Eng* 2012; 59: 2137–43.
28. Jeremy P, Tanya J, Daniel M. Advanced training in anaesthesia – the essential curriculum. Oxford: Oxford University Press; c2014. Chapter 21.6, Management of children with multiple injuries; p. 396-9.
29. Kärki S, Lekkala J. A new method to measure heart rate with EMFi and PVDF materials. *J Med Eng Technol* 2009; 33: 551–8.
30. Kärki S. Film-type sensor materials in measurement of physiological force and pressure variables [dissertation]. [Tampere]: Tampere University of Technology; 2009. 61 p.
31. Kim JH, Lee SM, Lee S-H. Capacitive monitoring of bio and neuro signals. *Biomed Eng Lett* 2014; 4: 142–8.
32. Kim Y, Yoo S, Han C, Kim S, Shin J, Choi J. Evaluation of unconstrained monitoring technology used in the smart bed for u-Health environment. *Telemed J E Health* 2011; 17: 435–41.

33. Kortelainen JM, van Gils M, Pärkkä J. Multichannel bed pressure sensor for sleep monitoring. Proceedings of 39th Computing in Cardiology Conference; 2012 Sep 9-12; Krakow, Poland. IEEE; c2012. p. 313-6.
34. Kristiansen J, Korshøj M, Skotte JH, Jespersen T, Søgaard K, Mortensen OS, Holtermann A. Comparison of two systems for long-term heart rate variability monitoring in free-living conditions: a pilot study. *Biomed Eng Online* 2011; 10: 27
35. Lee JS, Heo J, Lee WK, Lim YG, Kim YH, Park KS. Flexible capacitive electrodes for minimizing motion artifacts in ambulatory electrocardiograms. *Sensors* 2014; 14: 14732–43.
36. Li M, Kim YT. Development of patch-type sensor module for wireless monitoring of heart rate and movement index. *Sens Actuator A-Phys* 2012; 173: 277–83.
37. Lim YG, Hong KH, Kim KK, Shin JH, Lee SM, Chung GS, Baek HJ, Jeong D-U, Park KS. Monitoring physiological signals using nonintrusive sensors installed in daily life equipment. *Biomed Eng Lett* 2011; 1: 11-20.
38. Lim YG, Lee JS, Lee SM, Lee HJ, Park KS. Capacitive measurement of ECG for ubiquitous healthcare. *Ann Biomed Eng* 2014; 42: 2218-27.
39. Migliorini M, Kortelainen JM, Pärkkä J, Tenhunen M, Himanen SL, Bianchi AM. Monitoring nocturnal heart rate with bed sensor. *Methods Inf Med* 2014; 53: 308–13.
40. Moody GB, Mark RG, Goldberger AL. PhysioNet: a research resource for studies of complex physiologic and biomedical signals. Proceedings of Computers in Cardiology Conference; 2000; Sep 24-27; Cambridge, MA, USA. IEEE; c2000. p. 179–82.
41. Nash DB. Health 3.0. *Pharm Ther* 2008; 33: 69.

42. Niizeki K., Nishidate I, Uchida K, Kuwahara M. Unconstrained cardiorespiratory and body movement monitoring system for home care. *Med Biol Eng Comput* 2005; 43: 716–24.

43. Nishyama M, Miyamoto M, Watanabe K. Respiration and body movement analysis during sleep in bed using hetero-core fiber optic pressure sensors without constraint to human activity. *J Biomed Opt* 2011; 16: 017002.

44. Niskanen J-P, Tarvainen MP, Ranta-aho PO, Karjalainen PA. Software for advanced HRV analysis. *Comput Meth Prog Bio* 2004; 76: 73–81.

45. Pan J, Tompkins WJ. A real-time QRS detection algorithm. *IEEE Trans Biomed Eng* 1985; 32: 230–6.

46. Pantelopoulos A, Bourbakis NG. A survey on wearable sensor-based systems for health monitoring and prognosis. *IEEE Trans Syst Man Cybern Part C Appl Rev* 2010; 40: 1–12.

47. Patel S, Park H, Bonato P, Chan L, Rodgers M. A review of wearable sensors and systems with application in rehabilitation. *J NeuroEng Rehabil* 2012; 9: 21.

48. Shin JH; Chee YJ; Jeong D-U; Park KS. Nonconstrained sleep monitoring system and algorithms using air-mattress with balancing tube method. *IEEE Trans Inf Technol Biomed* 2010; 14: 147–56.

49. Singh D, Vinod K, Saxena SC, Deepak KK. Effects of RR segment duration on HRV spectrum estimation. *Physiol Meas* 2004; 25: 721–35.

50. Singh D, Vinod K, Saxena SC. Sampling frequency of the RR interval time series for spectral analysis of heart rate variability. *J Med Eng Technol* 2004; 28: 263–72.

51. Song M-H, Cho S-P, Kim W, Lee K-J. New real-time heartbeat detection method using the angle of a single-lead electrocardiogram. *Comput Biol Med* 2015; 59: 73–9.
52. Spinelli EM, Pallàs-Areny R, Mayosky MA. AC-coupled front-end for biopotential measurements. *IEEE Trans Biomed Eng* 2003; 50: 391–5.
53. Sztajzel J. Heart rate variability: a noninvasive electrocardiographic method to measure the autonomic nervous system. *Swiss Med Wkly* 2004; 134: 514–22.
54. Tamura T, Chen W. Seamless monitoring of physiological information in daily life: retrospectives and perspectives. *Adv Biomed Eng* 2015; 4: 86-95.
55. Tan X, Chen X, Hu X, Ren R, Zhou B, Fang Z, Xia S. EMD-based electrocardiogram delineation for a wearable low-power ECG monitoring device. *Can J Electr Comp Eng-Rev Can Genie Electr Inform* 2014; 37: 212–21.
56. Task Force of the European Society of Cardiology, The North American Society of Pacing and Electrophysiology. Heart rate variability standards of measurement, physiological interpretation, and clinical use. *Circulation* 1996; 93: 1043–65.
57. Thayer JF, Friedman BH, Borkovec TD. Autonomic characteristics of generalized anxiety disorder and worry. *Biol Psychiatry* 1996; 39: 255–66.
58. Tu Y, Fu X, Li D, Huang C, Tang Y, Ye S, Chen H. A novel method for automatic identification of motion artifact beats in ECG recordings. *Ann Biomed Eng* 2012; 40: 1917–28.
59. Ueno A, Yama Y. Unconstrained monitoring of ECG and respiratory variation in infants with underwear during sleep using a bed-sheet electrode unit. Proceedings of 30th Annual International IEEE EMBS Conference; 2008 Aug 20-24; Vancouver, Canada. IEEE; c2008. p. 2329-32.

60. Vital signs (body temperature, pulse rate, respiration rate, blood pressure) [Internet]. Washington: Johns Hopkins Medicine. Available from http://www.hopkinsmedicine.org/healthlibrary/conditions/cardiovascular_diseases/vital_signs_body_temperature_pulse_rate_respiration_rate_blood_pressure_85,P00866/
61. Wang C, Lu W, Narayanan MR, Redmond SJ, Lovell NH. Low-power technologies for wearable telecare and telehealth systems: a review. *Biomed Eng Lett* 2015; 5: 1–9.
62. Wang F, Zou Y, Tanaka M, Matsuda T, Chonan S. Unconstrained cardiorespiratory monitor for premature infants. *Int J Appl Electromagn Mech* 2007; 25: 469–75.
63. Wiard R M, Inan OT, Argyres B, Etemadi M, Kovacs GTA, Giovangrandi L. Automatic detection of motion artifacts in the ballistocardiogram measured on a modified bathroom scale. *Med Biol Eng Comput* 2011; 49: 213–20.
64. Zheng YL, Ding XR, Poon CCY, Lo BPL, Zhang H, Zhou XL, Yang GZ, Zhao N, Zhang YT. Unobtrusive sensing and wearable devices for health informatics. *IEEE Trans Biomed Eng* 2014; 61: 1538–54.
65. Zhu H, Dong J. An R-peak detection method based on peaks of Shannon energy envelope. *Biomed Signal Process Control* 2013; 8: 466–74.
66. Zidelmal Z, Amirou A, Adnane M, Belouchrani A. QRS detection based on wavelet coefficients. *Comput Meth Programs Biomed* 2012; 107: 490-6.
67. Zidelmal Z, Amirou A, Ould-Abdeslam D, Moukadem A, Dieterlen A. QRS detection using S-Transform and Shannon energy. *Comput Meth Prog Bio* 2014; 116: 1–9.
68. Zimetbaum P, Goldman A. Ambulatory arrhythmia monitoring choosing the right device. *Circulation* 2010; 122: 1629–36.

## 국문초록

# 무구속 센서를 이용한 생체정보의 분석:

## 로드셀을 이용한 영유아 심탄도 측정 및 패치형 전극을 이용한 심전도 측정


불규칙한 생활과 스트레스가 많은 현대인들에게 건강은 언제나 돌봐야 할 존재가 되었다. 과거에는 질환을 조기에 진단하고 치료하기 위한 기술이 주류를 이루었으나, 최근에는 자신의 생체 정보를 지속적으로 모니터링하여 항상 건강한 상태를 유지할 수 있도록 예방과 관리를 지원하는 기술로 관심이 집중되는 것도 이와 같은 맥락으로 해석할 수 있다. 본 연구는 무구속 센서를 이용한 심장박동 및 호흡운동의 지속적 모니터링에 대한 연구결과를 정리하여 기술한 것이다. 심탄도 측정기술과 심전도 측정기술은 각각 기계적인 방법과 전기적인 방법에 기반하여 심장 또는 호흡 활동을 측정하는데 보편적으로 이용되어온 기술이다.

먼저, 심탄도 측정기술을 이용하여 영유아의 생체정보를 모니터링 할 수 있는 시스템을 개발하였다. 영유아의 경우에는 상시적인 건강 상태 모니터링이 매우 중요함에도 불구하고 몸을 고정하거나 압박하는 것이 어렵기 때문에, 무구속 방식의 생체신호 측정시스템이 중요하게 이용될 수 있는 가능성이 기대되는 대상이다. 그러나 기존의 무구속 생체신호 측정 시스템에 대한 활용 연구들은 대부분 성인을 대상으로만 진행되어 왔다. 따라서, 로드셀 센서를 부착한 생체신호 측정 침대를 개발하였으며, 측정된 로드셀 신호에서 심장 박동 및 호흡 정보를 분리하는 알고리즘을 개발하여 영유아를 대상으로 유효성을 평가하였다. 개발된 시스템을 이용하여 6세 미만의 영유아 피험자를

대상으로 실험한 결과, 유용성있는 심장 박동 및 호흡정보를 분리할 수 있었으며, 상용화 장비와 비교했을 때에도 적정한 오차 범위의 생체정보를 얻을 수 있었다. 따라서 영유아를 대상으로 호흡 곤란 또는 심장 이상 여부의 지속적인 관찰뿐만 아니라 더 나아가 임상으로의 활용에 까지 심탄도 측정기술을 확대하여 활용할 수 있을 것으로 기대한다.

다음으로는 휴대성과 착용감을 향상시킨 초소형 및 경량의 심전도 측정 모니터링 장비를 제작하고 심박변이도를 분석하는 알고리즘이 포함된 소프트웨어를 개발하여 그 신뢰성에 대하여 검증하였다. 심전도 모니터링은 U-헬스케어의 대표적인 유형으로, 심장 활동 및 심혈관 관련 질병을 진단하기 위하여 임상에서 가장 보편적으로 사용되고 있다. 또한, 연속적인 심장 박동의 주기 변화 정도를 측정하는 심박변이도 분석은 급성 심근경색 등의 심혈관 질환 예측과 교감 및 부교감 신경의 균형을 정량적으로 측정할 수 있는 비침습적 생리지표로 이용되고 있다. 개발된 장비는 전극간의 거리를 최소화 시킨 패치형 전극을 이용하기 때문에 다수의 전극 부착으로 인한 사용자의 불편을 줄일 수 있었으며, 동잡음이 발생하는 상황에서도 보다 안정적으로 생체신호를 모니터링 할 수 있음을 확인하였다. 또한 정신적 스트레스를 유발한 상황에서의 심박변이도 분석의 유의미한 차이를 계산하여 자율신경계 불균형 상태를 나타낼 수 있었다.

정보통신기술과 의료기술을 융합하여 사용자에게 시간 및 공간적 제약이 없이 건강관리 및 의료서비스를 제공하는 무구속 센서 기반의 생체정보 분석 기술은 현대인의 건강 증진과 관리에 큰 도움을 줄 수 있다. 또한, 이러한 기술로 인해 사용자는 자신의 건강 상태를 지속적으로 모니터링 하면서 필요한 의료서비스를 적기에 제공받을 수 있으므로 최소의 의료서비스 비용으로도 삶을 질을 향상시킬 수 있을 것으로 기대된다.

**주요어**: 유헬스케어, 무구속 센서, 생체정보 분석, 휴대용 심전도 측정 장비, 영유아의 심탄도 측정, 심박변이도 분석, 피크 검출 알고리즘, 최적 센서 선택을 위한 자동 알고리즘, 스트레스 평가

**학 번:** 2011 – 30297

# Appendix

## Education

**• Ph. D.**

Interdisciplinary Program in Bioengineering

The Graduate School, Seoul National University

Academic adviser: Kwangsuk Park

Title of dissertation : Physiological Information Analysis Using Unobtrusive Sensors: BCG from Load-Cell Based Infants' Bed and ECG from Patch Electrode

**• Master & B. S.**

Department of Biosystems & Biomaterials Science and Engineering

College of Agriculture and Life Sciences, Seoul National University

## Publications

**[International Journals]**


1. **Lee WK**, Yoon H, Han C, Joo KM, Park KS. Physiological signal monitoring bed for infants based on load-cell sensors. *Sensors* 2016; 16: 409.
2. **Lee WK**, Yoon H, Park KS. Smart ECG monitoring patch with built-in R-peak detection for long-term HRV analysis. *Ann Biomed Eng* 2016; 44: 2292-301.
3. Lee JS, Heo J, **Lee WK**, Lim YG, Kim YH, Park KS. Flexible capacitive electrodes for minimizing motion artifacts in ambulatory electrocardiograms. *Sensors* 2014; 14: 14732-43.

4. Lee HJ, Hwang SH, Yoon H, **Lee WK**, Park KS. Heart rate variability monitoring during sleep based on capacitively coupled textile electrodes on a bed. *Sensors* 2015; 15: 11295-311.

**[Domestic Journals]**

1. **이원규**, 이홍지, 윤희남, 정기성, 박광석. 침대 패드 형태의 용량성 전극에서 측정된 심전도 신호를 처리하기 위한 자동 잡음 제거 및 피크 검출 알고리즘, *Journal of Biomedical Engineering Research*, 2014; 35: 87-94.
2. 이정수, **이원규**, 임용규, 박광석. 패치형 웨어러블 심전도 측정 시스템을 위한 접착성 폴리우레탄 기반의 용량성 전극, *Journal of Biomedical Engineering Research*, 2014; 35: 203-10.
3. 이정수, 이홍지, **이원규**, 임용규, 박광석. 비접촉 눈 깜박임 측정 안경형 디바이스를 이용한 실시간 스펠러의 구현, *Journal of Biomedical Engineering Research*, 2015; 36: 283-90.

## Patents

1. 심부 체온 모니터링을 위한 비침습 및 무구속적 단층 체온계
   김성민, 박광석, 심수영, 김한별, **이원규**, 유호석, 전효선
   등록번호: 10-1506075 (2015.03.19)
2. 뇌파측정을 통한 개인 인증 방법, 시스템 및 컴퓨터 프로그램
   박광석, 한정민, 김상경, 윤희남, **이원규**, 정다운
   등록번호: 10-1607432 (2016.03.23)

## Honors & Awards

1. Best Poster Award (최우수 포스터상)
   제 48회 대한의용생체공학회 추계학술대회 (2013년)
   논문제목: 음악에 의한 심혈관계 생체신호의 변화 분석
   이원규, 김상경, 윤희남, 정다운, 김고근, 박광석
2. Award in Idea Contest (일반부 우수상)
   한국과학기술단체 총연합회 주관 행복한 과학기술 공모전 (2014년)
   ALS 환자의 자유로운 의사소통을 위한 ITO 필름 기반 안경형 안구 움직임 측정 시스템 및 가상키보드 개발
   이정수, 이원규, 이홍지
3. Best Paper Award
   12th International Conference on Ubiquitous Healthcare, Japan; 2015.
   Paper entitled with "Effect of physical and mental conditions on nonlinear HRV analysis"
   **Wonkyu Lee**, Heenam Yoon, Kwangsuk Park

## Conference proceedings

**[International Conference]**

1. Sim SY, Jeon HS, Chung GS, Kwon SJ, **Lee WK**, Park KS. Fall detection algorithm for the elderly using acceleration sensors on the shoes. 33rd Annual International IEEE EMBS Conference, Boston, USA; 2011.
2. **Lee WK**, Chung GS, Baek HJ, Park KS. Heart sounds measurement using PVDF film sensor and their comparison with RR intervals of ECG signals, IEEE-EMBS International Conference on Biomedical and Health Informatics (BHI), Hong Kong and Shenzhen, China; 2012.
3. Sim SY, **Lee WK**, Baek HJ, Park KS. A nonintrusive temperature

measuring system for estimating deep body temperature in bed, 34th Annual International IEEE EMBS Conference, San Diego, USA; 2012.

4. **Lee WK**, Baek HJ, Sim SY, Park KS. Ballistocardiogram application for non-intrusive measurement monitoring Valsalva-induced hemodynamic changes on a chair, 9th International Conference on Ubiquitous Healthcare, Gyeongju, Republic of Korea; 2012.
5. Kim SK, Kim KK, **Lee WK**, Yoon H, Jung DW, Park KS. Dynamic relationship between cardiolocomotor coupling and cardiorespiratory coupling during walking on treadmill, 9th International Conference on Ubiquitous Healthcare, Gyeongju, Republic of Korea; 2012.
6. Sim SY, **Lee WK**, Jeon HS, Kim HB, Park KS. Simulation study of a newly designed structure for monitoring deep body temperature, 9th International Conference on Ubiquitous Healthcare, Gyeongju, Republic of Korea; 2012.
7. Lee JS, Baek HJ, Heo J, **Lee WK**, Park KS. A new paradigm of P300 based mental speller for reducing eye fatigue, 9th International Conference on Ubiquitous Healthcare, Gyeongju, Republic of Korea; 2012.
8. Kim HB, Lee HJ, Baek HJ, **Lee WK**, Lee JS, Park KS. A preliminary study of non-intrusive blood pressure monitoring using portable device, International Conference on BIOSTEC, Barcelona, Spain; 2013.
9. **Lee WK**, Lee HJ, Lee JS, Yoon H, Sim SY, Lim YG, Park KS. Validation of algorithm with noise tolerance methods to detect R-wave, 15th International Conference on Biomedical Engineering, Singapore; 2013.
10. **Lee WK**, Yoon H, Park KS. Patch-type ECG measurement system for daily life ANS activity monitoring, Mongolia-Korea Conference on Biomedical Applied Science and Engineering, Ulaanbaatar, Mongolia; 2014.

11. **Lee WK**, Ha YN, Yoon H, Park KS. ECG monitoring patch for non-invasive assessment of ANS, International Biomedical Engineering Conference jointly with uHealthcare 2014, Gwangju, Republic of Korea; 2014.
12. Yoon H, Hwang SH, **Lee WK**, Jung DW, Lee YJ, Jeong DU, Park KS. Heart rate estimation in ballistocardiogram acquired from various sensors, International Biomedical Engineering Conference jointly with uHealthcare 2014, Gwangju, Republic of Korea; 2014.
13. Han C, Kim SK, Yoon H, **Lee WK**, Park CS, Kim KK, Park KS. Contrast between spectral and connectivity features for electroencephalography based authentication, World Congress on Medical Physics & Biomedical Engineering, Toronto, Canada; 2015.
14. **Lee WK**, Yoon H, Jung DW, Hwang SH, Park KS. Ballistocardiogram of baby during sleep, 37th Annual International IEEE EMBS Conference, Milan, Italy; 2015.
15. **Lee WK**, Yoon H, Park KS. Method of ballistocardiogram measurement for infants, International Biomedical Engineering Conference, Gyeongju, Republic of Korea; 2015.
16. **Lee WK**, Yoon H, Park KS. Effect of physical and mental conditions on nonlinear HRV analysis, 12th International Conference on Ubiquitous Healthcare, Osaka, Japan; 2015.

**[Domestic Conference]**

1. 이원규, 정기성, 백현재, 박광석. PVDF 필름을 이용한 심음 (Heart Sound) 측정 기술, 제 44회 대한의용생체공학회 추계학술대회; 2011.
2. 심수영, 백현재, 이원규, 정기성, 김영석, 박광석. 변형된 구조의 dual heat flux thermometer을 이용한 심부 체온 추정,

제 44회 대한의용생체공학회 추계학술대회; 2011.

3. 윤희남, **이원규**, 허정, 박광석. 운동 중 심전도 측정에서 동잡음 자동 판단을 위한 파라미터 추출과 활용,
   제 45회 대한의용생체공학회 춘계학술대회; 2012.
4. **이원규**, 백현재, 윤희남, 심수영, 박광석. 심음 특성을 이용한 심탄도 신호의 분석, 제 46회 대한의용생체공학회 추계학술대회; 2012.
5. 백현재, **이원규**, 허정, 박광석. 맥파도달시간을 이용한 비가압 혈압추정을 위한 생체모델기반의 보정방법,
   제 46회 대한의용생체공학회 추계학술대회; 2012.
6. 심수영, 전효선, **이원규**, 박광석. uHealthcare를 위한 단층의 심부 체온 프로브 개발, 제 46회 대한의용생체공학회 추계학술대회; 2012.
7. 윤희남, 김상경, **이원규**, 정다운, 이유진, 정도언, 박광석. 수면단계에 대한 심폐 동기역학 특성 변화,
   제 46회 대한의용생체공학회 추계학술대회; 2012.
8. 김상경, 김고근, **이원규**, 윤희남, 정다운, 박광석. 보행 중 심박, 호흡, 움직임의 위상 동기역학적 특성 분석,
   제 46회 대한의용생체공학회 추계학술대회; 2012.
9. 김한별, 심수영, 심교식, **이원규**, 유호석, 박광석. 목걸이 형태의 심박수 모니터링 장치 개발,
   제 47회 대한의용생체공학회 춘계학술대회; 2013.
10. 유호석, 심수영, **이원규**, 박광석. Double Sensor를 이용한 일반 환경온도에서의 심부 체온 측정,
    제 47회 대한의용생체공학회 춘계학술대회; 2013.
11. 심수영, 유호석, **이원규**, 전효선, 박광석. 비침습 및 무구속적 연속 체온 모니터의 정확도 평가,
    제 47회 대한의용생체공학회 춘계학술대회; 2013.
12. **이원규**, 김상경, 윤희남, 정다운, 김고근, 박광석. 음악에 의한

심혈관계 생체신호의 변화 분석,

제 48회 대한의용생체공학회 추계학술대회; 2013.

13. 윤희남, 김상경, 김고근, **이원규**, 정다운, 이유진, 정도언, 박광석. 수면 심박-호흡의 위상 동기 특성과 방향성 관계 분석,

제 48회 대한의용생체공학회 추계학술대회; 2013.

14. **이원규**, 하용남, 윤희남, 김기언, 박광석. T-REX: 일상생활 중 심전도 모니터링을 위한 패치형 시스템,

제 49회 대한의용생체공학회 춘계학술대회; 2014.

15. 이정수, 허정, **이원규**, 임용규, 박광석. 운동중 심박수 측정을 위한 벨트형 용량성 전극 시스템,

제 49회 대한의용생체공학회 춘계학술대회; 2014.

16. **이원규**, 윤희남, 이홍지, 이정수, 박광석. 자동 잡음 제거 및 피크 검출 알고리즘의 성능 비교평가,

제 50회 대한의용생체공학회 춘계학술대회; 2015.

17. 한정민, 이정수, 김지훈, 윤희남, 김상경, **이원규**, 박광석. 단일 채널 뇌전도 기반 개인 인증 성능 평가,

제 50회 대한의용생체공학회 춘계학술대회; 2015.

18. 이정수, **이원규**, 이홍지, 임용규, 박광석. 안경형 비접촉 눈 깜박임 측정 디바이스와 깜박임 기반 실시간 스펠러,

제 50회 대한의용생체공학회 춘계학술대회; 2015.

19. 이홍지, **이원규**, 윤희남, 박광석. 다채널 심전도 시스템에서 접촉 채널 자동 검출방법,

제 51회 대한의용생체공학회 춘계학술대회; 2016.

20. 윤희남, 김상경, **이원규**, 정다운, 최재원, 이유진, 정도언, 박광석. 두 사람의 수면에서 나타나는 심박동의 상호작용,

제 51회 대한의용생체공학회 춘계학술대회; 2016.